3rd International WHEEL

WHEEL PJ

PrecambrianWorld 2024 in South Africa

7th International Geoscience Symposium

--The past,modern and future Earth : geologic, oceanic and biogenic processes over 4.6 billion years--

at JBS
Johannesburg Business School
University of Johannesburg

http://wheelaa.jp

JSPS 日本学術振興会 Japan Society for the Promotion of Science
研究拠点形成事業 Core-to-Core Program
Asia-Africa Science Platforms
科研費 KAKENHI

Name

Introduction

Thank you for participating in the 3rd WHEEL Symposium in Johannesburg. This event consists of two days of oral presentations (December 5–6) and a four-day field excursion (December 7–10). As this is the third symposium, many familiar faces are likely present. Let's ensure everyone's safety throughout the event.

Purpose of WHEEL

1. **Understanding Large-Scale Tectonics and Environmental Changes**

Prioritizing research and sample collection in areas with well-preserved strata from a particular era is crucial. Geological reconstruction of "fresh outcrop records and rock samples" combined with high-precision chemical analysis allows us to decipher environmental change records. Understanding Earth's history requires a comprehensive grasp of diverse local geology to reconstruct a global narrative. It is vital to collaborate with regions that host these outcrops, exchanging opinions and progressing toward a deeper understanding of Earth's history. Through discussions and joint research, we aim to lead the field of environmental reconstruction research through Earth's history.

2. **Fostering Training of Young Researchers**

In recent years, geology, especially research focused on fieldwork, has faced challenges such as inefficiency in labor and paper writing, and a lack of time within university education. This has resulted in a shortage of young researchers. To address this:

Developing Field Data Collection Skills: Young researchers should be actively sent to partner countries to acquire practical fieldwork skills at globally significant sites, skills that are difficult to obtain solely through current university education.

Training in Chemical and Age Data Analysis: There is a need to nurture researchers capable of analyzing and interpreting chemical and chronological data from crucial samples.

Additionally, we aim to enhance research skills for both parties by fostering communication among young researchers from various countries and by holding symposiums to build the foundation for future international scientific collaboration.

This symposium marks the third, following those held in Kochi and Cairo. As it is the final year, we hope it will lead to further advancements in research. We sincerely thank the participants from Egypt and South Africa for their invaluable cooperation.

3ed WHEEL Seminar
(7th IGS "Precambrian World 2024")

Dec 5-6, 2024

Symposium in University of Johannesburg

Arrival

O.R. Tambo international Airport Arrival place.

You should wait near the statue in the arrivals hall if you are being picked up. The statue is of Oliver Tambo.

- He was a key figure in the fight against apartheid in South Africa, and the airport is named in his honor.

- Currency Exchange Locations:
    - In this hall (banks and ATMs available).
    - ATMs near the hotel and in the supermarket district.
  - Current Exchange Rates (for 100R):
    - USD: $5.5–$5.6
    - Japanese Yen: ¥830
    - Ghanaian Cedi: 86 GHS
    - Egyptian Pound: 274–275 EGP
  - Payment Methods:
    - Credit cards are widely accepted in many locations.

- Locations

Red line shows to go the Agterplaas Guesthouse.
Pick line shows to go UJ (Geology department)

Map around conference area and UJ

1) Accommodation Dec 4-10th

Agterplaas Guesthouse
66 6th Avenue
Email: agterplaas@agterplaas.co.za


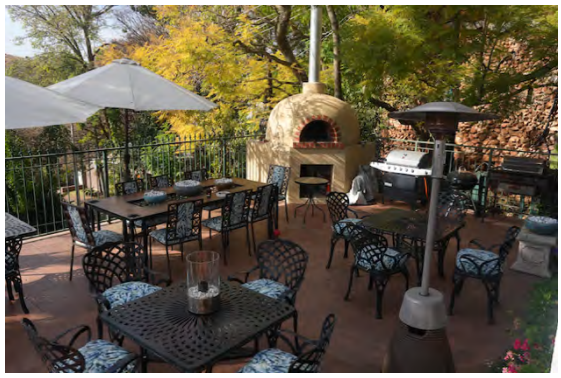

Guesthouse entrance, outside garden terrace.


Kitchin and rooms. Twin rooms with bathroom.

---

2) Meals

Breakfast is included, but Dinner is not included, so please prepare your own meals using supermarkets, restaurants, etc. A refrigerator is available, so you can buy supplies at a nearby supermarket.

Lunch will be prepared at a nearby restaurant. Please look forward to it! There is a nice Italian restaurant nearby where you can enjoy delicious pizza.

Alternatively, a shopping mall with a large supermarket called **Pick n Pay** is about a 10-minute walk away. You can have meals at a reasonable cost there. (Please make sure to return to the venue on time.)

While walking around the neighborhood

of the conference venue and the shopping mall is relatively safe during the daytime, you should avoid carrying and displaying valuables or a laptop computer.

3) Venue

The symposium venue is about a 15-minute walk (1.1 km) away from the Agterplaas Guesthouse and is managed by the Johannesburg Business School. It's a large venue shared with other groups, so please be mindful. On the day of the event, the location of the lecture rooms will be provided at the entrance.

For your presentations, **please bring your PowerPoint files on a USB drive**. We will transfer the data to the venue's computer in advance. For safety reasons, we do not recommend carrying personal computers with you.

Johannesburg Business School entrance gate and lobby.

4) Field Excursion

A separate guidebook will be distributed for the field excursion. Lunch will take place in small restaurants and in the form of picnics in the field. Besides the usual field gear please bring your own refillable water bottle. Tap water in Johannesburg is safe to drink – we will not provide bottled water.

5) Departure

Return flights will be discussed on-site. For those with early morning flights, arrangements will be made accordingly.

6) Climate

Currently, the lowest temperature is 11° C and the highest is 26° C due to a cold front. However, according to weekly forecasts, on the 6th, temperatures are expected to range from a minimum of 19° C to a maximum of 33° C. It is already summer, so there might be occasional showers. As it is inland, the temperature difference can be significant.

Timetable and Title

2024 Dec. 5						
9:00	9:10		Wellcome			
9:10	9:50	1	Axel	Hofmann	UJ	Factors Responsible For Witwatersrand Gold Mineralization
			rest			
10:00	10:20	2	Andrew	Kennedy	US	
10:20	10:40	3	Anna	Molekwa	Transvaal	Investigation Of The Neoarchaeach Carbonate Platform Formation And Diagenesis: A Case Study Of The Lime Acres Member In The Campellrand Subgroup, Griqualand West Sub-Basin, Transvaal Supergroup
10:40	10:50		rest morning tea			
10:50	11:10	4	Hanna	El Dokouny	Eg	Nb-Rich Biotite: A New Potential Source For Rare Metal Mineralization In Egypt
11:10	11:30	5	Mahyra	Tedeschi	Br	Unravelling The Protracted U-Pb Zircon Geochronogical Record Of High To Ultrahigh Temperature (Ht-Uht) Metamorphic Rocks
11:30	11:35		short rest			
11:35	11:40	6	Tathagata	Chowdhury	Biust	Raman Geothermometry Of Carbon Seams Of The Central Rand Group, Witwatersrand Basin, South Africa
11:40	11:45	7	Koki	Maegawa	JPN	Basic Observation Of The Upper Cretaceous Izumi Group At Eastern Area Of Kagawa Prefecture, Southwest Japan
11:45	11:50	8	Fezeka	Dliwako	Kaapvaal	Tectonic Processes Affecting The Central Kaapvaal Craton
12:00	14:00		lunch			
14:00	14:30	9	Manuel	Reinhardt	BARB3	Traces Of Microbial Diversity 3.42 Billion Years Ago (Buck Reef Chert, Barberton Greenstone Belt)
14:30	14:50	10	Thatayaone	Oletile	Bots	Petrological, Geochemical Characterization And U-Pb Zircon Dating Of (Meta)-Granitoids From The Beit Bridge Complex Of The Limpopo Belt In Botswana.
14:50	15:10	11	Isaac	Ajigo	NIGERIA	Geochemistry And Geochronology Of The Igarra Schist Belt Of Nigeria: Insights Into Paleoproterozoic Crustal Evolution.
15:10	15:20		rest afternoon tea			
15:20	15:50	12	Shoichi	Kiyokawa	Aust	Detailed Observation Of Siderite Iron Formation Of The 3.1 Ga Cleaverville Formation, Coastal Pilbara Terrane, Western Australia
15:50	16:20	13	Carlos	A. Rosière	Br	The Eastern Border Of The Southern Espinhaço Rang
16:20	16:30		rest			
16:30	16:50	14	Fatma	A. E. Mousa	Eg	Quaternary Fossilized Spring Calcareous Tufa Of The Kharga Oasis (Western Desert, Egypt): Sedimentary Records Of Past Humidity In The Eastern Sahara
16:50	17:10	15	Maher	Dawoud	Eg	The Evolution Of Sinai And The North Eastern Desert Segments Through Rifting During The Initiation Of The Pan-African Orogeny

2024 Dec. 6

9:10	9:40	16	**Frank**	**Nyame**	GH	Occurrence And Geological Setting Of A Neoproterozoic Ironstone In The Buem Structural Unit (Bsu), Ghana
9:40	9:50		rest			
9:50	10:10	17	**Kwabina**	**Ibrahim**	GH	Mineralogical And Geochemical Signature Of Gold Mineralization At Esaase Mine, Akroma Gold, Northeastern Axim-Konongo (Ashanti) Belt, Ghana: Implications For Mining And Environmental Management
10:10	10:30	18	**Samuel**	**Nunoo**	GH	Textural And Isotopic (Δ13C And Δ34S) Records From Carbonaceous Sedimentary Rocks From The Paleoproterozoic Birimian Of Nw Ghana, West Africa: Implication On Potential Gold Source
10:30	10:40		rest morning tea			
10:40	11:00	19	**Satoshi**	**Yoshimaru**	GH	Reconstruction Of The Stratigraphic And Structural Development History Of The Paleoproterozoic Birimian Belt In The Cape Three Points Area, Southwestern Ghana
11:00	11:20	20	**Kwame**	**Fynn**	GH	The Geology Of Gold Mineralization In The Nangodi Greenstone Belt, Ne Ghana
11:20	11:30		rest			
11:30	12:00	21	**Ion**	**Francovschi**	Baltica	Accessing The Ediacaran-Cambrian Boundary In Sw Baltica Based On Shrimp And Ca-Id-Tims Zircon U-Pb Dates
12:00	14:00	Lunch				
14:00	14:40	22	**Andrey**	**Bekker**	US	Tracing Oxidative U Cycle With Pb Isotopes In Marine Carbonates
14:40	14:50		rest			
14:50	15:10	23	**Kento**	**Motomura**	Bar	Nitrogen Cycling In The Paleoarchean Ocean
15:10	15:30	24	**Niraj**	**Buhyan**	India	Boron Isotope Composition In Tourmaline From Paleoproterozoic Pb-Zn Deposits Of Aravalli-Delhi Fold Belt: Implications For Source Of Ore-Forming Hydrothermal Brines In Sedex And Mvt Deposits
15:30	15:40		rest afternoon tea			
15:40	16:00	25	**Kazuyasu**	**Shindo**	Botswana	Preliminary Investigation Of Cu Mineralization In Matsitama, Northeastern Botswana
16:00	16:20	26	**Satoshi**	**Tonai**	JPN	Relationship Between Load Cycle And Deformation In Sand-Wedge Experiments
16:20	16:30		rest			
16:30	16:50	27	**Mohamed**	**Abouelhassan**	Eg	Challenges And Solutions: Stratigraphic Delineation And Sedimentological Facies Analysis Of Incised-Valley Fill Reservoirs
16:50	17:20	28	**Sharad**	**Master**	Senegal	Palaeoproterozoic High Δ13C Carbonates From The Mako Supergroup, Eastern Senegal: A First Record Of The Lomagundi Carbon Isotope Excursion In West Africa

FACTORS RESPONSIBLE FOR WITWATERSRAND GOLD MINERALIZATION

Axel Hofmann

Department of Geology, University of Johannesburg, Johannesburg, South Africa.
ahofmann@uj.ac.za

The exceptional gold mineralization in quartz pebble conglomerates of the Witwatersrand Basin is attributed to a combination of factors. These factors are linked to the co-evolution of the atmosphere, hydrosphere, lithosphere and biosphere, at a very specific time in Archaean geological history and the evolution of the Kaapvaal Craton. Following craton stabilization and its subaerial emergence, intense chemical weathering and erosion of large volumes of granitoid-greenstone basement released detrital and dissolved gold. Shallow-marine reworking in a long-lived and slowly subsiding basin subjected to episodic compressional deformation and relative sea-level oscillations led to sedimentary concentration of detrital gold. The interaction between acidic, anoxic, and sulfurous surface runoff and more oxidizing marine waters in a near-coastal oxygen oasis supported microbially mediated diagenetic pyrite formation and incorporation of dissolved gold in the pyrite crystal lattice. Erosion and reworking of diagenetic pyrite gave rise to detrital pyrite that characterize most reefs. Abundance of detrital uraninite in conglomerates, derived from erosion of Mesoarchaean granites, and episodes of hydrocarbon migration through sedimentary strata during deep burial set the scene for further enhancement of gold grades in the reefs. Granular and seam pyro-bitumen formed by radiation-induced polymerization of hydrocarbons around detrital uraninite. Gold dissolved in migrating hydrothermal fluids was then reduced and precipitated upon interaction with the reef pyro-bitumen during hydrothermal placer modification.

INVESTIGATION OF THE NEOARCHAEACH CARBONATE PLATFORM FORMATION AND DIAGENESIS: A CASE STUDY OF THE LIME ACRES MEMBER IN THE CAMPELLRAND SUBGROUP, GRIQUALAND WEST SUB-BASIN, TRANSVAAL SUPERGROUP

Mmasetena Anna Molekwa[1,2], Robert Bolhar[3], and Zubair Jinnah[4]

1. School of Geosciences, University of the Witwatersrand, Johannesburg, South Africa,
amolekwa@uj.ac.za
2. Department of Geology, University of Johannesburg, Johannesburg, South Africa.
3. School of Geosciences, University of the Witwatersrand, Johannesburg, South Africa,
robert.bolhar@wits.ac.za
4. School of Geosciences, University of the Witwatersrand, Johannesburg, South Africa,
Zubair.Jinnah@wits.ac.za

1. Introduction

The 1500 and 1700 m thick, Neoarchaean (2.55 to 2.64 Ga) (Barton et al., 1994; Beukes and Gutzmer, 2008) Campbellrand Subgroup was deposited during a time when the intra-cratonic Griqualand West sub-basin in the Transvaal Supergroup was experiencing its highest subsidence rates in the central part, which was matched by the accumulation of carbonates (Beukes, 1987; Altermann and Wotherspoon, 1995). It is a dolomite-dominated succession comprising chiefly stromatolitic dolomites intercalated with cherts, shales and minor siliciclastic rocks. The top part of the Campbellrand Subgroup consists of crinkly algal mats interbedded with laminated sapropelic dolomites of Kogelbeen Formation and dolomitic domal stromatolites with finger-like bifurcating columnar microstructure of Gamohaan Formation (Eriksson et al., 2006).

Between the dolomite-dominated Kogelbeen and Gamohaan Formations occurs the ca. 110 m thick Lime Acres Member, which is a remarkably well-preserved, stromatolitic limestone succession that has great potential to reconstruct the ancient surface conditions and holds important clues as to when and how dolomitization occurred. Previous studies have not indicated whether the unit has been dolomitized or never underwent dolomitization.

The morphological, microstructural and geochemical investigation of the lithofacies of the Lime Acres Member and their relationship with surrounding sedimentary lithofacies are employed to reconstruct the depositional environments.

2. Results

The limestone lithofacies in the Lime Acres Member include stratiform, domal and columnar stromatolites, massive micrite, fenestral carbonate mudstone and microbial boundstone, which represent supratidal to upper intertidal depositional environments. Middle-lower intertidal to shallow subtidal deposits consist of planar-laminated, planar cross-bedded sandy limestones, oolitic grainstone, columnar stromatolite and oncolite. Deep subtidal deposits consist of black shale, which commonly marks the base shallowing-upward cycles. Fenestral laminites represent a shelf-lagoonal depositional environment. The limestones of Lime Acres Member contain stromatolites that consist

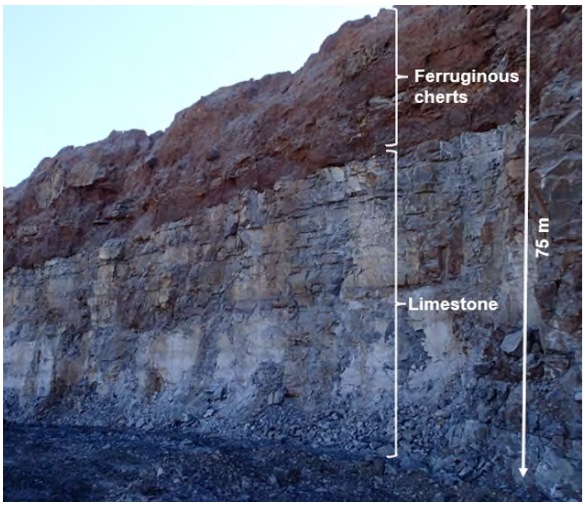

Figure 1. Limestone unit of the Lime Acres Member overlaid by a ferruginous chert unit.

of an alternation of micritic and microsparitic laminae. Microbialites with various morphologies are observed, including planar laminae (stromatolites), oncoids roll-up structures, calcified microbes, bedded cuspated microbialites, plumose structures, and net-like microbialites. SEM-EDS maps show that the Lime Acres Member limestones contain ca. 95% calcite with small to no amounts of detrital material. Although Lime Acres Member is a limestone-rich unit, dolomite is present but rare. Elemental and mineral phase maps obtained by SEM-EDS analysis using a Tescan-integrated-mineral-analyser (TIMA) show that dolomite is restricted to stratiform and cross-cutting veins. These dolomite veins have angular clasts of the limestone host rock, which may indicate that the veins were generated by hydraulic fracturing.

Matrix-selective dolomitization and evidence of dedolomitization are also observed in some parts of the stratigraphy, suggesting limestone could have been dolomitized and the dolomite reacted with solutions with a high Ca (super ++)/Mg (super ++) ratio forming calcium carbonate. Trace element data allow an investigation of aspects of carbonate depositional environments and ambient seawater compositions. Shale-normalized rare earth element (REE) distribution patterns of limestones exhibit positive La_{SN}, Gd_{SN} and YSN anomalies, superchondritic Y/Ho ratios and depleted light rare earth elements (LREEs) relative to the heavy rare earth elements (HREEs), which resemble the modern seawater composition. Dolomite samples have slight positive Gd anomalies which is a tetrad effect seen in seawater compared to limestone. Ce_{SN} is not anomalous in both limestones and dolomites suggesting deposition of limestones in anoxic conditions with no effect of later post-Great Oxygenation Event (GOE) fluid infiltration. Eu_{SN} is not consistent in all lithofacies; however, it is more enriched in limestone than dolomite, suggesting that the hydrothermal input was minimal.

3. Discussion

The sedimentological and petrographic examination reveals a cyclic shallowing-upward pattern, reflecting sea level variations during the deposition of the Lime Acres Member. The lamination suggests that carbonate precipitation occurred in situ within microbial mats. Trace element geochemical data of Lime Acres Member are consistent with open ocean vs isolated shallow marine (i.e., lagoon). Non-seawater REE patterns in dolomite and calcite pore- and vein-fillings likely reflect redistribution of rare earth elements during post-depositional alteration and/or reflect differences in the elemental and REE compositions of diagenetic fluids.

References

Altermann, W., and Wotherspoon, J.M.D. (1995) The carbonates of the Transvaal and Griqualand west sequences of the Kaapvaal Craton, with special reference to the Lime Acres Limestone deposit. *Miner Depos.* **30**, 124-134.

Barton, E.S., Altermann, W., Williams, I.S., and Smith, C.B. (1994) U-Pb zircon age for a tuff in the Campbell Group, Griqualand West Sequence, South Africa: Implications for Early Proterozoic rock accumulation rates. *Geology* **22**, 343-346.

Beukes, N.J. (1987) Facies relations, depositional environments and diagenesis in a major Early Proterozoic stromatolitic carbonate platform to basinal sequence, Campbellrand Subgroup, Southern Africa. *Sediment. Geol.* **54**, 1-46.

Beukes, N.J and Gutzmer, J. (2008) Origin and paleoenvironmental significance of major iron formations of the Archean Paleoproterozoic boundary. *Econ. Geol.* **15,** 5-47.

Eriksson, P.G., Altermann, W., and Hartzer, F.J. (2006) The Transvaal Supergroup and its precursors. In *The Geology of South Africa* (eds., M.R. Johnson, et al.), Geological Society of South Africa and Pretoria, Council for Geoscience, pp. 237-260.

NB-RICH BIOTITE: A NEW POTENTIAL SOURCE FOR RARE METAL MINERALIZATION IN EGYPT

Mohamed A. Abdelkader[1,2] *, Yasushi Watanabe[1], Maher Dawoud[2], Shogo Aoki[1], Carmela Tupaz[1], Yoshiaki Kon[3], Takuya Echigo[1], Hanaa A. El-Dokouny[2]

1. Mineral Resources and Tectonics Group, Department of Earth Resources Science,
Graduate School of International Resource Sciences, Akita University, Akita, 010-8502, Japan.
2. Department of Geology, Faculty of Science, Menoufia University, Gamal Abd El Nasr St., Shebin El-Kom 32958, Menoufia, Egypt
3. Geological Survey of Japan, National Institute of Advanced Industrial Science and Technology (AIST), Tsukuba, Ibaraki 305-8567, Japan

1. Introduction

Niobium (Nb) and tantalum (Ta) are strategic critical metals with substantial economic applicability. However, they are encountering a substantial supply risk due to their limited occurrence in a small number of countries (Schulz et al., 2017). The primary sources of Nb and Ta deposits include peralkaline granites, peraluminous granites, pegmatites and carbonatites (Linnen et al., 2012; Mackay and Simandl, 2014). Beside Nb and Ta economic potentiality, Nb/Ta ratio of a melt is an advantageous marker to track magmatic fractionation and the resulting compositional changes (López-Moro et al., 2017; Zhu et al., 2019) as they found as twins due to their similar physical and geochemical properties (Shannon and Prewitt, 1969). In evolved magmatic systems, Ta-Nb-bearing oxides were considered the principal controllers of both Nb–Ta fractionation and their concentrations in the residual melt (Linnen et al., 2013). Nevertheless, recent work has indicated that biotite, muscovite, and amphibole possess the capability to selectively fractionate Ta from Nb in granitic melts. Around 90% of Nb mining production comes from pyrochlore, and the rest comes from other oxide minerals such as columbite group minerals (Linnen et al., 2013). This study emphasizes the exceptionally high concentrations of Nb-Ta-Sn in biotite from rare metal-bearing biotite-rich granites of Umm Naggat area, central Eastern Desert, Egypt and establishes the genetic link between biotite and the secondary rare metal enrichment. These findings have the potential to illuminate biotite as a new potential source of Nb-Ta-Sn metals.

2. Results

The Umm Naggat pluton (UMNG) in Egypt is composed of rare metal bearing amphibole biotite granite (SBTG) in its southern sector and mica albite granite (NABG) in its northern sector. The SBTG rocks are predominantly composed of K-feldspar (~16-62.6 %), quartz (~31-47.8 %), plagioclase (~1-43 %), and biotite (± amphibole) (~12 %), with biotite being more abundant than amphibole. Zircon, fluorite, thorite, columbite, fergusonite, Fe-Ti oxides, and apatite are the most common primary accessory minerals. In contrast, chlorite, muscovite, fluorite, kaolinite, rutile, ilmenite, euxenite, and columbite are the main secondary minerals formed as a result of alteration. The NABG rocks are classified as alkali feldspar granite mainly consists of albite (~ 32-42%), quartz (~ 25-36%), K-feldspar (~ 24-34%), and mica (~ 1-7%). Amphibole and biotite in the SBTG crystallized from Nb-enriched magma and represent primary HFSE reservoirs in the SBTG. Primary amphibole from the SBTG contains Nb (280 ppm), Ti (5760 ppm), Y (506 ppm), Zr (87 ppm), and Mn (2801ppm), while biotite from the UMNG (SBTG and NABG) contains significantly higher Nb (1630 ppm), Ta (83 ppm), Sn (392 ppm), Ti (9268 ppm), Rb (2846 ppm), and Li (6331 ppm) contents. Biotite and amphibole contribute to ~53.5% and ~10.5% of the total Nb budget within the SBTG, respectively. The increasing Si, F, Rb, Li, Nb, and Cs and decreasing Mn, Ti, Fe, Sn, and Ta contents within the biotite of the SBTG to NABG indicate crystal fractionation toward the north in the UMNG.

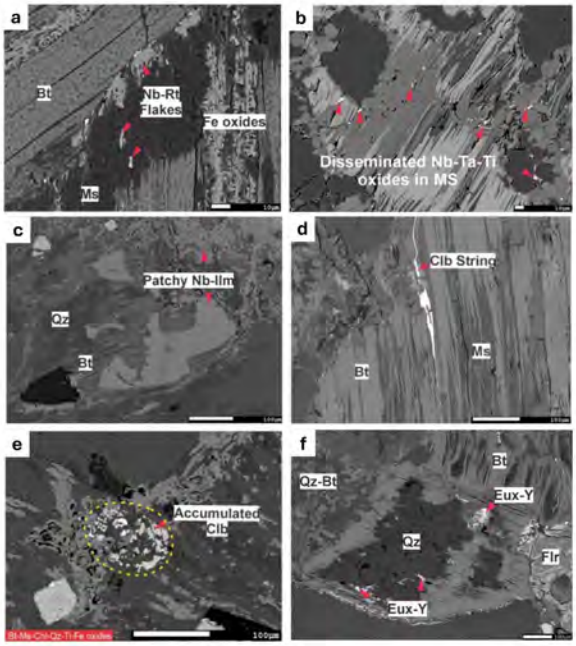

Figure 1. BSE in SBTG a) small flakes of Nb-rich rutile included within secondary muscovite after biotite, b) very fine disseminated grains of secondary Nb-Ta-Ti-rich phases within the hydrothermal muscovite and chlorite, respectively, c) patchy secondary Nb-ilmenite overgrowing the host biotite due to alteration, d) Columbite-Fe string extends along the cleavage of biotite parallel to secondary muscovite lamellae, e) fine-grained aggregations or accumulations of columbite embedded in biotite, muscovite, chlorite, secondary quartz and Ti-Fe oxides, f) the alteration-formed Nb-Y-Ti-REE oxides (euxenite) within biotite intergrown with secondary quartz and muscovite after biotite. Ms=muscovite, Bt=biotite, Chl=chlorite, Rt=rutite, Ilm= ilmenite, Clb=columbite, Qz=quartz, Eux-Y= euxenite-Y, Flr=fluorite,

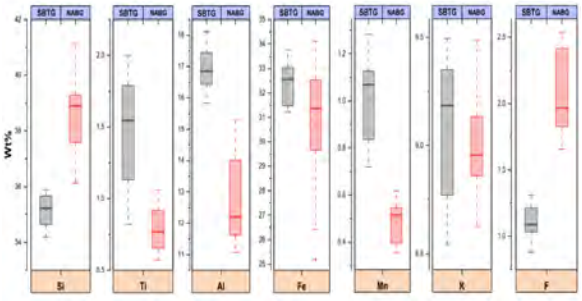

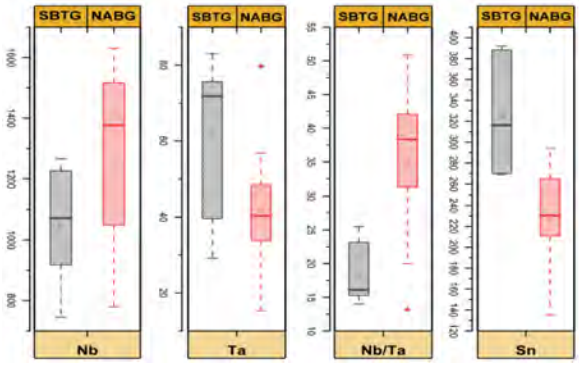

Figure 2. Comparative boxplot binary diagram highlighting the main difference in the concentration of the major and trace elements between the southern biotite (NBGs) and northern biotite (NABGs) in the Umm Naggat pluton.

3. Discussion

In the SBTG, hydrothermal alteration is divided into the metasomatic stage and aqueous stage.

The metasomatic fluid was enriched in F and Na, causing albitization and leading to the precipitation of secondary fluorite, columbite, and zircon. Biotite is extensively altered during the aqueous stage, mainly to muscovite and chlorite, through a paired dissolution-precipitation mechanism. The replacement textures of the primary mafic minerals imply that the hydrothermal fluids were hydrolytic and fluorine-bearing, resulting in the remobilization of Ta, Nb, W, Sn, Li, Ca, Y, and REE. During the alteration, Ti, Ta, Nb, and Fe were liberated from the biotite into the fluid as Ta-Nb-F complexes. The consumption of F during the formation of secondary fluorite and muscovite made the complexes unstable, resulting in the precipitation of secondary Ta-Ti-Nb-Y-REE-bearing phases near and within muscovite and chlorite forming Nb-Ta-Sn-bearing rutile, ilmenite, columbite, and euxenite that are significantly abundant in Nb, Ta, and Sn, compared to their primary equivalents (primary rutile, ilmenite, columbite, and fergusonite). The substantial increase in Nb, Ta, and Sn concentrations in the alteration-formed minerals indicates that the decomposition of biotite led to notable rare metal enrichment in the secondary minerals. Considering its distinctive petrography, mineralogy, and textural variations, the metasomatic Nb-Ta-Sn-rich mineralization may delineate a new potential source for rare metals in Egypt and worldwide.

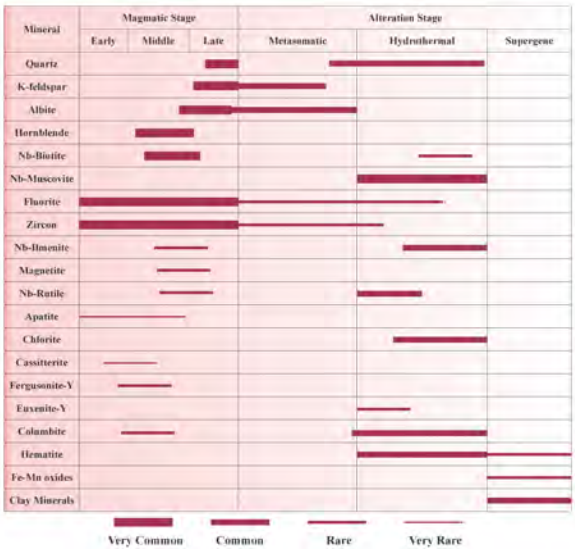

Figure 3. A general summary of the significant mineral paragenesis in the Umm Naggat biotite granites (SBTG) based on microscopic and SEM-BSE imagery observations.

References

Linnen, R., Samson, I., Williams-Jones, A., Chakhmouradian, A., 2013. Geochemistry of the rare-earth element, Nb, Ta, Hf, and Zr deposits, Treatise on Geochemistry: Second Edition, pp. 543-568.

Linnen, R.L., Van Lichtervelde, M., Černý, P., 2012. Granitic pegmatites as sources of strategic metals. Elements 8, 275-280.

López-Moro, F.J., Polonio, F.G., González, T.L., Contreras, J.L.S., Fernández, A.F., Benito, M.C.M., 2017. Ta and Sn concentration by muscovite fractionation and degassing in a lens-like granite body: The case study of the Penouta rare-metal albite granite (NW Spain). Ore Geology Reviews 82, 10-30.

Mackay, D.A., Simandl, G.J., 2014. Geology, market and supply chain of niobium and tantalum—a review. Mineralium Deposita 49, 1025-1047.

Schulz, K.J., Piatak, N.M., Papp, J.F., 2017. Niobium and tantalum. US Geological Survey. Hickman, A.H. (1983) *Geology of the Pilbara Block and its environs*. Geological Survey of Western Australia, Bulletin 127, 268p.

Shannon, R.T., Prewitt, C.T., 1969. Effective ionic radii in oxides and fluorides. Acta Crystallographica Section B: Structural Crystallography and Crystal Chemistry 25, 925-946.

Zhu, Z.-Y., Wang, R.-C., Marignac, C., Cuney, M., Mercadier, J., Che, X.-D., Charles, N., Lespinasse, M., 2019. Petrogenesis of Nb–(Ta) aplo-pegmatites and fine-grained granites from the Early Cretaceous Huangshan rare-metal granite suite, northeast Jiangxi Province, southeast China. Lithos 346, 105150.

UNRAVELLING THE PROTRACTED U-PB ZIRCON GEOCHRONOGICAL RECORD OF HIGH TO ULTRAHIGH TEMPERATURE (HT-UHT) METAMORPHIC ROCKS

Mahyra Tedeschi[1,2], Pedro Leonardo Rossi Vieira[2], Matheus Kuchenbecker[3], Bruno V. Ribeiro[4], Vitor Barrote[5], Humberto Reis[6], Laura Stutenbecker[7], Cristiano Lana[8], Antonio Pedrosa-Soares[2], Ivo Dussin[9]

1. Geological Survey of Finland, Helsinki, Finland; mahyra.tedeschi@gtk.fi, mahyratedeschi@gmail.com
2. Programa de Pós-graduação em Geologia da Universidade Federal de Minerais, Centro de Pesquisas Manoel Teixeira da Costa, Institute of Geosciences, Federal University of Minas Gerais, Belo Horizonte, Brazil; pedro.leonardo@gmail.com; pedrosasoares@gmail.com
3. Laboratório de Estudos Tectônicos, Universidade Federal dos Vales do Jequitinhonha e Mucuri, Diamantina, Brazil; matheusk@ict.ufvjm.edu.br
4. School of Earth, Atmosphere and Environment, Monash University, Victoria 3800, Australia; bruno.vieiraribeiro@curtin.edu.au
5. Paul Scherrer Institut, Villigen PSI Switzerland; vitor.barrote@psi.ch
6. Departamento de Geologia-Escola de Minas, Universidade Federal de Ouro Preto 35400-000, Brazil; reis.humbertols@gmail.com
7. School of Earth and Planetary Sciences, Curtin University, Perth, WA 6845, Australia; vitorbarrote@hotmail.com
8. Department of Materials and Earth Sciences, Institute of Applied Geosciences, TU Darmstadt, Germany; laura.stutenbecker@uni-muenster.de
9. TEKTOS Geotectonic Research Group, Geology Institute, Rio de Janeiro State University, Rio de Janeiro, Brazil; ivodusin@yahoo.com.br

1. Introduction

The assessment of detrital zircon age records is a key method in basin analysis, but it is prone to several biases that may compromise accurate sedimentary provenance investigations. High to ultrahigh temperature (HT-UHT) metamorphism (especially if T > 850 °C) is a natural cause of bias in provenance studies based on U-Pb detrital zircon ages, since zircon from rocks submitted to these extreme and often prolonged conditions frequently yield protracted, apparently concordant, geochronological records. Such age spreading can result from disturbance of the primary U-Pb zircon system, likewise from (re)crystallization processes during multiple and/or prolonged metamorphic events (Fig. 1). We used available geochronological data of HT-UHT metamorphic rocks acquired by different techniques (SIMS and LA-ICP-MS) and showing distinct compositions combined to new data from migmatites to demonstrate HT-UHT metamorphism may result in modes and age distributions of unclear geological meaning.

2. Results

The disturbance caused by HT-UHT metamorphism may induce misinterpretations on U-Pb detrital zircon provenance analyses. In most of the reported HT-UHT metamorphic rocks with protracted geochronological records, the zircon dataset registers a minimum U-Pb date corresponding to the age of the last metamorphic event according to interpretations. Thus, the inferred maximum depositional age based on U-Pb detrital zircon derived from the erosion of a HT-UHT metamorphic source is meaningful, since the sedimentation is subsequent to the closure of the U-Pb system within concordant zircon. The effects on the inferred maximum depositional age are of particular concern when the HT-UHT metamorphism affects the sedimentary rock that is the object of study, rather than a rock that would be the source of a sediment. In this case the original detrital zircon dates distribution could have shifted modes that might not directly represent the geological ages recorded by the source rocks. Furthermore, the real tectono-thermal events that were experienced by the source

rocks would likely be significantly underrepresented or even obliterated.

3. Discussion

To evaluate the presence of HT-UHT metamorphism-related bias in the detrital zircon record, we suggest a workflow for data acquisition and interpretation, combining a multi-proxy approach with: (i) in situ U-Pb dating coupled with Hf analyses to retrieve the isotopic composition of the sources, and (ii) the integration of a petrochronological investigation to typify fingerprints of the HT-UHT metamorphic event.

Our workflow allows to the appraisal of biases imposed by HT-UHT metamorphism and resulting disturbances in the U-Pb detrital zircon record, particularly for sedimentary rocks that underwent HT-UHT metamorphism and, finally, suggests ways to overcome these issues. The thorough discussion is present in Tedeschi et al. (2023).

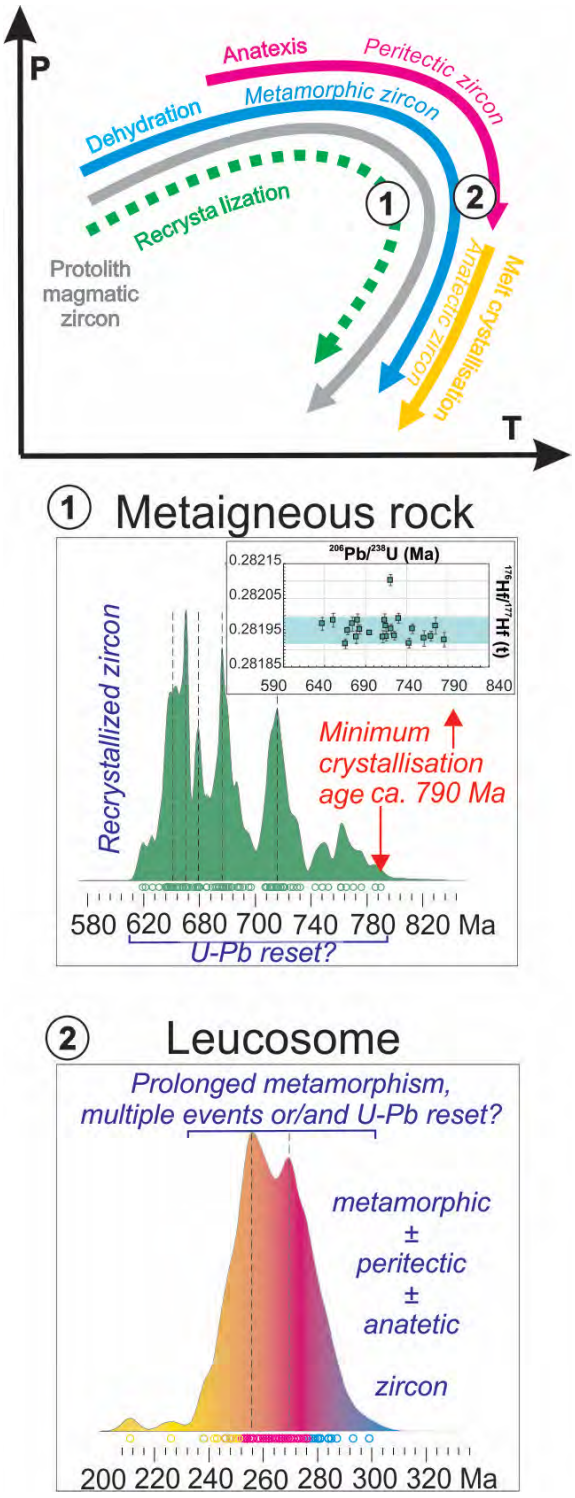

Figure1: Schematic cartoon summarizing potential zircon formation and recrystallization events during metamorphism (grey trajectory), the respective resulting zircon textures visible in cathodoluminescence images, and their U-Pb zircon record in probability density plots. (A) Growth of zircon under different pressure, temperature, and fluid conditions. Zircon recrystallization can occur

along the whole pressure–temperature path, strongly controlled by the availability of fluids. Fluid-absent systems result in solid-state recrystallization, while metasomatic and dissolution recrystallization occur in the presence of fluid (adapted from Chen and Zheng, 2017; the blue path for subsolidus, pink for peritectic, and yellow for anatectic reactions). (1) Zircon $^{206}Pb/^{238}U$ date spectrum of a single Neoproterozoic metamorphosed igneous rock exhibiting a protracted record of concordant grains with partial preservation of igneous textures and Hf isotopic signatures. Besides the presence of several dates modes lacking geological meaning (dashed vertical lines) the rock has only one geological meaningful age of ca. 790 Ma, interpreted as the minimum crystallization age. The protracted record is attributed to post-crystallization U-Pb disturbance (recrystallization, corresponding to the green path in A; Metaopdalite C8382 from Tedeschi et al., 2018). (2) Zircon $^{206}Pb/^{238}U$ date spectrum of zircon with metamorphic textures from a Cambrian migmatite (Paragneiss IZ-405 from Kunz et al., 2018) showing a protracted record with two dates modes. The spreading of U-Pb data from Kunz et al. (2018) is herewith interpreted as likely representing one or more mechanisms of resetting and neocrystallization (the coloured areas and circles through the detrital zircon spectrum represent the predominance of each of the processes from A in a neocrystallization scenario). Figure from Tedeschi et al. (2023).

References

Chen, R.-X., Zheng, Y.-F (2017) Metamorphic zirconology of continental subduction zone. J. Asian Earth Sciences **145**, 149–176.

Kunz, B.E., Regis, D., Engi, M. (2018) Zircon ages in granulite facies rocks: decoupling from geochemistry above 850 °C?. Contribution to Mineralalogy and Petrology**173**, 26.

Tedeschi, M., Pedrosa-Soares, A.C., Dussin, I., Lanari, P., Novo, T., Pinheiro, M.A., Lana, C., Peters, D. (2018) Protracted zircon geochronological record of UHT garnet-free granulites in the Southern Brasília orogen (SE Brazil): Petrochronological constraints on magmatism and metamorphism. *Precambrian Research*, **316**, 101-126.

Tedeschi, M., Rossi Vieira, P.L., Kuchenbecker, M., Ribeiro, B.V., Barrote, V., Reis, H., Stutenbecker, L., Lana, C., Pedrosa-Soares, A., Dussin, I. (2023) Unravelling the protracted U–Pb zircon geochronological record of high to ultrahigh temperature metamorphic rocks: Implications for provenance investigations. Geoscience Frontiers, **14** (2), 101515.

RAMAN GEOTHERMOMETRY OF CARBON SEAMS OF THE CENTRAL RAND GROUP, WITWATERSRAND BASIN, SOUTH AFRICA

Tathagata Roy Choudhury[1], and Axel Hofmann[2]

1. Department of Geology, University of Johannesburg, APK Campus, South Africa
tathagata.roy.chowdhury@gmail.com
2. Department of Geology, University of Johannesburg, APK Campus, South Africa
ahofmann@uj.ac.za

1. Introduction

The application of Raman spectroscopy to the study of Carbonaceous Matter (CM) is an important non-destructive method to understand the thermal evolution of sedimentary strata. Transformation of CM in metasedimentary rocks has long been considered an important indicator of peak conditions of the metamorphic cycle[1]. The Archean Witwatersrand Basin in South Africa hosts several auriferous 'reefs' that typically contain carbonaceous matter as pyrobitumen grains (fly-speck carbon) or lamina (carbon seams). While the basin received significant attention for its gold mineralization, the questions on the origin, emplacement, and maturation of the CM are still open to debate. This study presents the results of Raman spectroscopic analysis of the CM in the Central Rand Group to understand the mineralogical heterogeneity and to quantify the peak metamorphic temperatures. The Raman spectra of the CM from 38 samples of different reefs covering the entire Central Rand Group were obtained using a WITec alpha300R Confocal Laser Raman microscope equipped with an automated sample stage for micro-Raman mapping (Assore Raman Lab, University of Johannesburg, South Africa).

2. Results

The Raman spectrum of CM consists of first-order (1100–1800 cm^{-1}) and second-order (2500–3100 cm^{-1}) regions, with the first-order region being the most important and is characterized by the G- and D-bands[2]. The width of the D- and G-band decreases with progressive metamorphism[1]. The peak fitting protocol determined the spectral parameters in which Raman spectra were deconvoluted into five (5) smaller bands. The heterogeneity and structural order of the samples can be assessed through the difference in relative positions of different peaks in different reefs. The Raman spectra for both massive pyrobitumen and fly-speck carbon are remarkably similar across all localities. In the first-order region of the Raman spectra, the D- and G-bands are observed as having strong intensities (Fig. 1). The well-pronounced D1 band is situated at ~1347 cm^{-1} with a FWHM of ~156 cm^{-1}. The weak D2 band with an FWHM of ~22 cm^{-1} is observed at ~1620 cm^{-1}. The D3 band is a broad peak found at ~1496 cm^{-1} with a large area (FWHM ~262 cm^{-1}) and weak intensity. The D4 band is also broad with much lower intensity, situated at ~1246 cm^{-1}. The G-band is frequently observed as the peak with the highest intensity. It is often narrow with a FWHM value of ~77 cm^{-1}. A general directly proportional relationship between the ratios of R2 varying between 0.55 and 0.7 and D1/G ranging between 0.8 and 1.0 is observed.

The CM maturation temperature can be calculated from the intensity ratios of different peaks[1]. An evaluation of the peak metamorphic temperature obtained from various samples shows little variation. The average results yielded temperatures around 360 ˚C (±50˚C).

3. Discussion

The evolution of both ratios is similar, with a low dispersion of points indicating the reliability of these parameters as indicators of the degree of organization of the carbonaceous matter. It is, however, important to point out that (1) the uncertainty is generally lower with R2 than D1/G, and (2) very poorly organized carbonaceous matter exhibits low values for the D1/G ratio owing to the very broad D1 band with lower intensity[1]. This study identifies little heterogeneity among carbonaceous seams and a similar average temperature of maturation of the CM consistent with the previous studies indicating greenschist facies metamorphism for the Witwatersrand Basin[3].

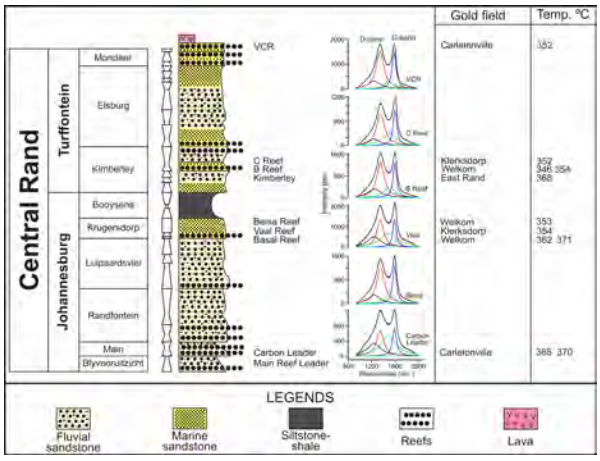

Figure 1. Raman spectra of carbonaceous matter of the Central Rand Group of the Witwatersrand Basin.

References

1. Beyssac, O., Goffé, B., Chopin, C. and Rouzaud, J.N., 2002. Raman spectra of carbonaceous material in metasediments: a new geothermometer. Journal of Metamorphic Geology, 20(9), 859-871.
2. Nemanich, R.J. and Solin, S.A., 1979. First-and second-order Raman scattering from finite-size crystals of graphite. Physical Review B, 20(2), 392.
3. Phillips, G.N., 1987. Metamorphism of the Witwatersrand gold fields: conditions during peak metamorphism. Journal of Metamorphic Geology, 5(3), 307-322.

Basic observation of the Upper Cretaceous Izumi Group at Eastern area of Kagawa prefecture, South West Japan

KOKI MAEGAWA[1], SHOICHI KIYOKAWA[1,]

1. Department of Earth and Planetary, Faculty of Science, KYUSHU University (JAPAN)

maegawa.koki.551@s.kyushu-u.ac.jp

kiyokawa@geo.kyushu-u.ac.jp

Introduction

The Upper Cretaceous Izumi Group is located in the southwestern inner belt of Japan along the prominent "Median Tectonic Line (MTL)." This group was deposited on granite associated with the Ryoke Belt, formed during the Lower Cretaceous (86.0 ± 1.2 Ma, based on U–Pb dating in western Kagawa Prefecture; Nakajima et al., 2004). The Izumi Group extends approximately 300 km in length and 15 km in width, as observed on geological maps, exhibiting a highly elongated shape. This morphology suggests that the Izumi Group basin formed as a pull-apart basin caused by the strike-slip movement of the Median Tectonic Line (Taira et al., 1983).

The deposition age of the Izumi Group is estimated to be 78.3 ± 0.5 Ma (U–Pb dating), corresponding to the Middle Campanian, as determined using radiolarian biostratigraphy (Noda and Kurihara, 2016). Despite significant research on the basin's formation, its origin remains unresolved.

The Izumi Group was divided into three main sections:

1. Basal conglomerate unit
2. Thick mudstone unit
3. Alternating beds of mudstone and sandstone unit

The basal conglomerate unit is alternating beds well rounded pebbly conglomerate and shale (Yamasaki, 1986). The thickness and lithology of the basal conglomerate vary significantly laterally.

A primary objective of this study is to investigate this lateral variation through detailed fieldwork, including geological mapping, columnar section construction, and profiling. By analyzing these changes, the study aims to determine their geological significance. Furthermore, the relationship between the middle mudstone section and the upper alternating beds is currently unclear. This research seeks to reconstruct the basin's formation, paleo-topography, and depositional environment across all units.

Results

This study identified four stratigraphic units in our research area:

1. Arkose sandstone and black mudstone unit (lowest; ~0–50 m thick)
2. Thick conglomerate unit (lower; ~130 m thick)
3. Thick mudstone unit (middle; ~600 m thick)
4. Thick sandstone unit (alternating beds of sandstone and mudstone; >700 m thick).

The basal conglomerate is underlain by an arkose sandstone and black mudstone unit, which lies directly on an unconformity with the granite. This basal arkose sandstone unit is new defined as basal unit, whose thickness around 20-50 m in thickness and lithology vary depending on the location.

Discussion

The conglomerate layer appears to have formed in a channel-like system, as evidenced by the orientation of gravel long axes and the erosional contact with the underlying sandstone. This indicates that the depositional environment of the Arkose sandstone and black mudstone and conglomerate units was a river or shallow marine channel system. There are trace fossils with in black shale sequence.

The thick mudstone unit, characterized by alternating beds of sandstone and mudstone, is interpreted as a relative silent condition oceanic condition.

In this location above unconformity, sedimentary environment shows subaerial to shallow silent condition oceanic condition preserved. Then thick sandstone sediment overlie on the muddy condition silent basin.

Future work include tracking the evolution of the strike-slip-related sedimentary basin by analyzing variations in the distribution of the lower thick conglomerate layer above granitic basement. Additionally, we aim to investigate the origin of the arkosic sandstone and angular conglomerate derived

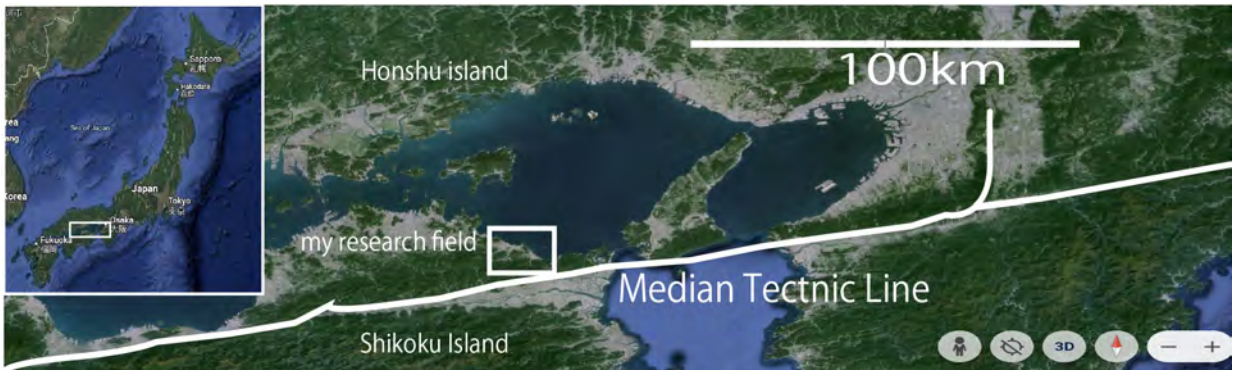

Figure1 Location map: Study area is located Eastern portion of Shikoku Island.

from granite, as well as the black shale layer deposited arkosic sandstone. By examining the overlying conglomerate layer, we intend to clarify the relationship between fluvial activity along the eastern margin of the Eurasian continent at that time and the strike-slip related sedimentary fore arc basin.

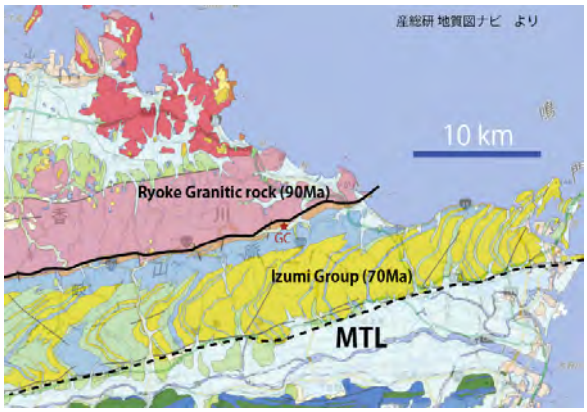

Figure 2 Overview geologic map of the Izumi Group at east Kagawa prefecture.

Figure 3 There are sandstone beds in thick conglomerate layer. Low section in HIKETA coast.

References

Hashimoto, H., Ishida, K., Yamasaki, T., Tsujino, Y., and Kozai, T. (2015) Revised radiolarian zonation of the Upper Cretaceous Izumi inter-arc basin (SW Japan). Revue de Micropaléontologie, vol. 58, no. 1, p. 29–50.

Nakajima, T., Kamiyama, H., Williams, I. S., and Tani, K. (2004) Mafic rocks from the Ryoke Belt, southwest Japan; implications for Cretaceous Ryoke/San-yo granitic magma genesis. Transactions of the Royal Society of Edinburgh: Earth Sciences, vol. 95, p. 249–263

野田 篤・栗原敏之 (2016) 四国東部観音寺地域の和泉層群から産出した後期白亜紀放散虫化石群集. 地調研報. vol. 67, p. 119–131.

Yamasaki, T. (1986) Sedimentological study of the Izumi Group in the northern part of Shikoku, Japan. Science Reports of the Tohoku University, 2nd Series, Geology, vol. 56, p. 43–70.

Taira, A., Saito, Y., and Hashimoto, M. (1983) The role of oblique subduction and strike-slip tectonics in the evolution of Japan. In Hilde, T. W. C. and Uyeda, S. eds., Geodynamics of the Western Pacific–Indonesian Region, Geodynamics Series, vol. 11, American Geophysical Union, p. 303–316.

Tectonic processes affecting the central Kaapvaal craton

Fezeka Dliwako[1], Karen Smit[2], and Linda Iaccheri[3]

1. School of Geosciences, University of the Witwatersrand, Johannesburg, South Africa.
   2320205@students.wits.ac.za
2. School of Geosciences, University of the Witwatersrand, Johannesburg, South Africa.
   karen.smit@wits.ac.za
3. School of Geosciences, University of the Witwatersrand, Johannesburg, South Africa.
   linda.iaccheri@wits.ac.za

1. Introduction

The Kaapvaal Craton in southern Africa is one of the best-preserved ancient environments for studying early Earth processes (e.g., Anhaeusser, 2014). Existing knowledge of the evolution of the Archaean Kaapvaal comes primarily from studies on the Barberton granite-greenstone terrane and the Ancient Gneiss Complex. The central Kaapvaal craton has received significantly less attention compared to its peripheral regions, leaving gaps in our understanding of its formation and evolution.

This study aims to address these gaps by investigating the age and evolution of the central Kaapvaal Craton. This will be done through analysing TTG gneisses from the Johannesburg Dome and rare peridotitic xenoliths that were sampled by the Roberts Victor kimberlite upon ascent. The age of lithospheric mantle will primarily be determined using Lu-Hf isotopes of garnets from the Roberts Victor peridotites, along with Pb-Pb and Rb-Sr isotopes in clinopyroxene. Crystallisation ages of the Johannesburg Dome TTGs will be determined through U-Pb isotopes in zircons. These crustal ages will be supplemented by Sm-Nd and Lu-Hf isotopes on a subset of whole-rock powder samples in order to shed light on the timing of crustal formation and the potential protolith of the TTGs.

2. Results

Preliminary results from Roberts Victor show that the xenoliths have transitional pyroxenitic-lherzolitic assemblages, similar to the compositions of Voorspoed diamond mineral inclusions (Viljoen *et al.*, 2018). Calculated pressures and temperatures range between 2.8 GPa and 5.2 GPa and 681 and 1021 °C, yielding a lithospheric thickness of 220–230 km below the central Kaapvaal. Age dating of these xenoliths will allow us to know whether the lithosphere attained this thickness during Archaean craton formation, or later during lithospheric evolution. Similar to previous reports, these Roberts Victor peridotites are extremely altered and contain abundant serpentine, calcite, and quartz. Eight xenoliths contain peridotitic garnets with 19.5–21.5 wt.% MgO, 3.2–7.1 wt. % Cr_2O_3 and 4.17–6.22 wt. % CaO. Garnets from 6 of these 8 xenoliths classify as lherzolitic (G9), with a garnet from 1 xenolith classifying as harzburgitic (G10), and a garnet from 1 xenolith classifying as high-TiO2 peridotitic (G11). Garnet from two xenoliths (G10 and G9) have sinusoidal REE_N patterns with maxima at Sm_N, whereas the remainder of the garnets have broadly 'normal' REE_N patterns that are depleted in $LREE_N$, with flat to slightly fractionated $MREE_N$ to $HREE_N$.

Clinopyroxene in these eight xenoliths have Na/(Na+Ca) that range between 0.09 and 0.31 and molar Cr/(Cr+Al) between 23.9 and 49.6. These compositions are transitional between Cr-diopside and omphacite, similar to the compositions of clinopyroxene inclusions in Voorspoed diamonds that were found to be 'transitional websteritic-lherzolitic'.

One xenolith contains pyroxenitic (G4) garnet with 21 wt.% MgO, 0.4 wt. % Cr_2O_3 and 3.89 wt. % CaO. Clinopyroxene in this xenolith has Na/(Na+Ca) of 0.21 and molar Cr/(Cr+Al) of 3.75, classifying as omphacite.

The 29 TTG samples from the Nooitgedacht Platform of the Johannesburg Dome have metaluminous to peraluminous whole-rock compositions (Anhaeusser, 1999), and overall have similar compositions to TTGs from worldwide

Archaean granite-greenstone terranes. The Nooitgedacht TTGs are characterised by being silica-rich (SiO_2 ~70 wt.%), aluminous (Al_2O_3 ~15 wt.%), with high Na_2O (3–7 wt.%) and a Na_2O/K_2O ratio greater than 1 (Anhaeusser, 1999; Van Tonder and Mouri, 2010). The Nooitgedacht TTGs exhibit $LREE_N$ enrichment and $HREE_N$ depletion relative to chondrite composition and this indicates metasomatism, TTGs in Archaean localities worldwide show this REE pattern relative to chondrite composition.

3. Discussion

The preliminary results from Roberts Victor and Nooitgedacht reveal crucial insights into the central Kaapvaal Craton's mantle and crustal evolution. The Roberts Victor xenoliths, with their transitional pyroxenitic-lherzolitic assemblages and garnet types (G9, G10, G11), indicate a complex mantle history involving melt depletion and metasomatic enrichment. The calculated pressures and temperatures (2.8–5.2 GPa, 681–1021 °C) suggest a lithospheric thickness of 220–230 km, key for cratonic stability. The clinopyroxene compositions align with Voorspoed diamond inclusions, supporting a shared mantle evolution.

The Nooitgedacht TTGs' high silica, aluminum content, and Na_2O/K_2O ratios reflect typical Archaean crust formation, enriched in LREE and depleted in HREE, indicating metasomatic processes. These findings suggest that both mantle and crust experienced significant modifications through subduction or mantle interactions, essential for the craton's prolonged stability. Age dating will clarify if these features originated during craton formation or later, contributing to broader Archaean tectonic models.

Investigating the specific age relationships between the mantle roots of cratons and their overlying crust will help constrain the mode of craton formation (Pearson *et al.*, 2021), whether at convergent margins, within a stagnant or partially mobile lid, and with either plume and/or subduction geochemical signatures. This study aims to shed light on the tectonic processes that shaped the heart of the Kaapvaal Craton and the continental assembly and tectonic events that influenced this ancient part of southern Africa.

References

Anhaeusser, C.R. (1999) Archaean crustal evolution of the central Kaapvaal Craton, South Africa: evidence from the Johannesburg Dome. *South African Journal of Geology*, **102(4)**, 303-305.

Anhaeusser, C.R. (2014) Archaean greenstone belts and associated granitic rocks–a review. *Journal of African Earth Sciences*, **100**, 685-713.

Van Tonder, D.M. and Mouri, H. (2010). Petrology and geochemistry of the granitoid rocks of the Johannesburg Dome, central Kaapvaal Craton, South Africa. *South African Journal of Geology*, **113(3)**, 257-286.

Viljoen, K.S., Perritt, S.H. and Chinn, I.L. (2018). An unusual suite of eclogitic, websteritic and transitional websteritic-lherzolitic diamonds from the Voorspoed kimberlite in South Africa: Mineral inclusions and infrared characteristics. *Lithos*, **320**, 416-434.

TRACES OF MICROBIAL DIVERSITY 3.42 BILLION YEARS AGO (BUCK REEF CHERT, BARBERTON GREENSTONE BELT)

Manuel Reinhardt[1], Volker Thiel[1], Axel Hofmann[2], Jan-Peter Duda[1], Joachim Reitner[1], and Henrik Drake[3]

1. University of Göttingen, Department of Geobiology, Göttingen, Germany manuel.reinhardt@uni-goettingen.de
2. University of Johannesburg, Department of Geology, Johannesburg 2006, Republic of South Africa
3. Linnæus University, Department of Biology and Environmental Science, Kalmar, Sweden

1. Introduction

Microorganisms inhabited Earth already in the Paleoarchean (3.6–3.2 Ga ago), but the structure and complexity of early ecosystems is still a matter of debate. Here we investigated four carbonaceous cherts from the ca. 3.42-billion-year-old Buck Reef Chert, Barberton greenstone belt (Barberton Drilling Project core BARB3, see Hofmann (2024) for details), to assess potential microbial activity in the ancient environment (Reinhardt et al. 2024). The chert precursors were deposited as primary silica precipitates in a back-arc basin, and trapped abundant carbonaceous matter (CM). The CM and associated mineral phases (here siderite and pyrite) were investigated using various macro- and micro-scale analytical techniques, including scanning electron microscopy, micro-X-ray fluorescence, Raman spectroscopy, secondary ion mass spectrometry, and catalytic hydropyrolysis followed by gas chromatography-mass spectrometry.

2. Results and discussion

The carbonaceous matter (CM) is exceptionally well preserved (Fig. 1), resulting from rapid silicification (Reinhardt et al., 2024). Geothermometry based on Raman spectra of the CM suggests a peak metamorphic overprint to lower greenschist facies (Reinhardt et al., 2024), which is in line with an entrapment before regional metamorphosis around 3.2 Ga. The CM pool can therefore be considered as syngenetic. Bulk $\delta^{13}C$ analyses indicate that the main CM pool derives from anoxygenic phototrophic primary producers. Microscale $\delta^{13}C$ measurements on CM associated with pyrite, together with multiple sulfur isotope analyses of these pyrites, however, suggest the presence of microbial sulfate reduction in the ancient ecosystem (Reinhardt et al., 2024). Additionally, microscale $\delta^{13}C$ signals of CM associated with siderite indicate methanogen-methanotroph and/or acetogen-acetotroph couples (Reinhardt et al., 2024). Together, these results highlight a metabolic diversity in parts of the Paleoarchean Buck Reef Chert environment, and reflect an already advanced biological carbon cycle during these early times (Reinhardt et al., 2024).

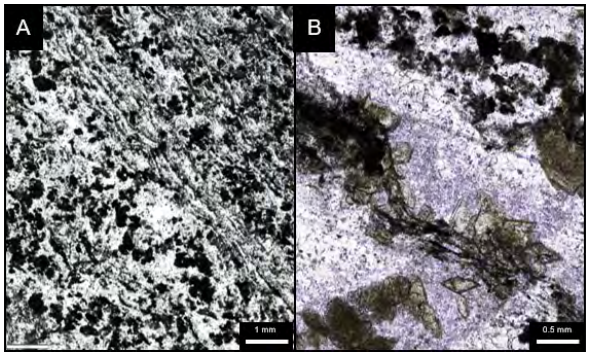

Figure 1. Carbonaceous matter (CM) appearance in the analyzed cherts. (A, B) The CM (black) is typically preserved in sedimentary layers as well-rounded clots or ultra-fine particles in thin laminae draping the material below. In some layers, CM appears in close association with siderite (light brown crystals in B).

References

Hofmann, A. (2024). The Barberton Drilling Project's Buck Reef Chert core BARB3 – Sedimentary facies and depositional environment of a 3.4 Ga marine platform succession. Precam. Res., 414, 107584.

Reinhardt, M., Thiel, V., Duda, J.-P., Hofmann, A., Bajnai, D., Goetz, W., Pack, A., Reitner, J., Schanofski, M., Schönig, J., Whitehouse, M.J., and Drake, H. (2024). Aspects of the biological carbon cycle in a ca. 3.42-billion-year-old marine ecosystem. Precam. Res., 402, 107289.

PETROLOGICAL, GEOCHEMICAL CHARACTERIZATION AND U-PB ZIRCON DATING OF (META)-GRANITOIDS FROM THE BEIT BRIDGE COMPLEX OF THE LIMPOPO BELT IN BOTSWANA.

Thatayaone Oletile[1], Alexander Proyer[1], Fulvio Franchi[2,3]

1. Department of Mineral Resources, Botswana International University of Science and Technology
oletilet@biust.ac.bw

2. Dipartimento di Scienze della Terra e Geoambientali, Università degli studi di Bari – aldo Moro, Bari, Italy, School of Geoscience

3. University of the Witwatersrand, Johannesburg, South Africa

1. Introduction

Twenty-two samples of (meta)-granitoids, from the Botswana part of the Central Zone of the Limpopo Belt were characterized petrographically, and by major and trace element geochemistry. In addition, U-Pb age information was obtained by LA-ICP-MS analysis from separated zircons. The granitoids were partly migmatitic and partly affected by later alkali-metasomatism.

2. Results & Discussion

Geochemically, the rocks can be subdivided into high-HREE (heavy rare earth elements) TTGs (tonalite-trondhjemite-granodiorite), low-HREE TTGs and one sanukitoid following TTG subdivision by Halla et al. (2009). High-HREE TTGs exhibit high silica content (68.5-71.7 wt.%), high $\Sigma(HREE)_N$ of (57.56-442.74), lower Strontium content (120.31-341.90 ppm), and negative Eu anomalies ($Eu/Eu^* = 0.47-0.91$), suggesting they originated from partial melting of metabasalts transformed into garnet amphibolite under low-pressure conditions possibly with mantle involvement. Low-HREE TTGs on the other hand show high silica content (68.5-71.7 wt.%), low values of $\Sigma(HREE)_N$ of (17.29-50.69), less pronounced Eu anomalies and low Yb_N (1.31-4.05) suggesting they are derived from a metabasaltic source under high-pressure conditions (plagioclase-poor garnet amphibolite or eclogite). The medium-HREE granitoid (sanukitoids) is characterised by low silica content (55.77 wt. %), a moderate value of $\Sigma(HREE)_N$ (224.13), high MgO = 1.35 wt% (Mg# = 34), K_2O = 2.15 wt% and Ba + Sr = 881 ppm suggesting the sanukitoid magma likely resulted from partial melting of a metasomatized mantle wedge peridotite in a subduction zone setting.

The age information of eleven selected (meta)-granitoids reveals a complex scenario, with most the granitoids emplaced between 2561 ± 11 to 2685 ±21 Ma indicating that the dominant period of crustal growth was in the Neoarchean. Specifically, low-HREE were emplaced between 2685 ± 21 Ma to 2606 ± 13 Ma and high-HREE between 2640 ± 5.27 to 2600 ± 8 Ma with sanukitoids notably, emplaced at 2607 ± 4 Ma marking the onset of subduction process (existence of a mantle wedge through which the magma passes). One sample (19-OT-12) constrains a major metasomatic event in the area at 1906 ± 150 Ma, while another sample, a garnet bearing (meta)-granitoid (19-OT-07A), which intruded as a sheet along the margin of metasedimentary rocks in a tightly folded closed structure, was emplaced at 2592 ± 10 Ma, provides a maximum age of both high-grade gneissic foliation and development of the tightly folded meta sedimentary structure. The granitoids also records zircon ages ranging between 2421 ± 27 and 2574 ± 13 Ma which were interpreted as a result of protracted thermal activity after the 2.6 Ga main igneous episode. This event also marks the migmatisation of the granitoids. Additionally, the inherited zircon ages from older crust ($^{207}Pb/^{206}Pb$ ages ranging between 3020 ± 29 and 2773.7 ± 11.5 Ma) implying some reworking of the Mesoarchean crust.

References

Halla, J., van Hunen, J., Heilimo, E., & Hölttä, P. (2009). Geochemical and numerical constraints on Neoarchean plate tectonics. Precambrian Research, 174 (1–2), 155–162.

GEOCHEMISTRY AND GEOCHRONOLOGY OF THE IGARRA SCHIST BELT OF NIGERIA: INSIGHTS INTO PALEOPROTEROZOIC CRUSTAL EVOLUTION.

Isaac Ajigo, Axel Hofmann, Marlina Elburg

Department of Geology, University of Johannesburg, South Africa
iajigo@uj.ac.za; ahofmann@uj.ac.za; marlinae@uj.ac.za

1. Introduction

The metasedimentary belts of Nigeria are geographically restricted to the western half of the country. One of them is the Igarra schist belt, located at the extreme south of this region. The Igarra schist belt has been a centre of attraction to many researchers because of its resources such as gold, marble as well as other reported metallic ore mineralization such as chalcopyrite and magnetite. As part of the Nigerian basement complex, the Igarra schist belt consists of low-grade metasedimentary rocks, unconformably overlying gneissic granitoids with which they are infolded; they have been intruded by Pan-African granitoids. The supracrustal metasedimentary cover consists predominantly of quartzite, quartz-muscovite-schist, quartz-chlorite/biotite schist, calc-silicate gneiss, marble and metaconglomerate. Limited availability of geochemical and geochronological data has hampered the understanding of the tectonic framework and evolution of this belt. Investigated rocks from the Igarra schist belt include selected lithological units from both the granitoids and the metasedimentary units. Analytical techniques deployed for this purpose include major element analyses using X-ray fluorescence (XRF), Inductively Coupled Plasma Mass spectrometry (ICP-MS) analyses for trace element composition as well as Laser Ablation (LA)-ICP-MS for U-Pb zircon analyses.

2. Results

Investigated granitoids surrounding the Igarra schist belt include the Ibillo grey gneiss, Dagbala granite gneiss and the Igarra granite, whereas metasedimentary rocks include quartz schist, biotite schist and metaconglomerate.

In the total alkali-silica (TAS) plot (SiO_2 vs Na_2O+K_2O; after Cox et al., 1979), the Dagbala granite gneiss and Igarra granite plot in the granite field while the grey gneiss plots as quartz diorite. All the granitoids plot in the field of calc-alkaline series in the AFM discriminant diagram (after Irvine and Barager, 1971). They plot in the peraluminous field in the $Al_2O_3/CaO+Na_2O+K_2O$ vs Al_2O_3/Na_2O+K_2O (Al-index discriminant after Maniar and Piccoli, 1989), plot. The granitoids plot as orthogneiss in the MgO vs Al_2O_3 ratio plot (after Marc, 1992) and as high K calc-alkaline series in the SiO_2 vs K_2O plot (after Peccerillo and Taylor, 1976). Trace elements (Y vs Nb after Pearce et al., 1984) plot characterizes granitoids of Igarra schist belt as being of volcanic arc granite (VAG) and syncollisional granite (syn-COLG) affinities while Co vs Th plot (after Hastie et al., 2007) characterizes them as high-K calc-alkaline and shoshonite series. Rare earth element (REE) patterns of the granitoids indicate negative anomaly of Eu, Ba, Ti, Nb, Ta, Sr and positive anomaly of Li, Rb, Ce, Pb and Th.

All the metasedimentary rocks, except quartz schist, plot as wacke in the Log (SiO_2/Al_2O_3) vs Log (Fe_2O_3/K_2O) discrimination plot (after Herron, 1988); quartz schist plot as subarkose. Also in the source material discriminant (DF1 vs DF2) plot for major elements (after Roser and Korsch, 1988), the Igarra metasediments are spread between quartzose sedimentary and felsic igneous provenance while in the K_2O/Na_2O vs SiO_2/Al_2O_3 diagram (after Maynard et al., 1982), they are spread between active and passive continental margin. In the trace elements discrimination plots, the Igarra metasedimentary rocks plot midway between early Archean mudstone and post-Archean shale in the V vs Cr plot (after Floyd et al., 1989) and felsic sources in the La/Sc vs Th/Co plot (after Cullers, 2002). Rare earth element (REE) distribution pattern for the Igarra metasediments indicate negative anomaly with respect to Eu, Ti, Sr, Ba, Nb and Ta and positive anomaly with respect to Li, Pb and Sc.

U-Pb zircon age data for granitoids in the Igarra schist belt indicate 555 ± 11 and 2262 ± 22 Ma as lower and upper concordia intercepts respectively for the grey gneiss (MSWD = 0.67). Dagbala granite gneiss gives lower and upper intercepts of 588 ± 13

and 2259 ± 25 Ma respectively with MSWD = 2.3. The Igarra granite on the other hand gives a single concordia intercept of 599.8 ± 7.1 (MSWD =1.14). This is taken as the crystallization age of the granite. Detrital zircon data for the metasedimentary rocks of the Igarra schist belt indicate a maximum depositional age of approximately 1500 Ma for the metaconglomerate. The dominant age group for this rock lies between 2000 and 3000 Ma while the approximate maximum depositional age lie outside this range. For the quartz schist, the approximate maximum depositional age is 1000 Ma, which lies outside the dominant age group of approximately 2000 Ma. The biotite schist on the other hand forms two age clusters with the approximate maximum depositional age of 700 Ma associating with the minor cluster while the major cluster represent the dominant age population that lies approximately within 1500 and 2500 Ma.

3. Discussion

Geochemical characteristics of gneisses associated with the Igarra schist belt indicate high-K, calc-alkaline, peraluminous orthogneisses, derived from protoliths of VAG and syn-COLG affinities. Negative anomaly of Ba, Nb and Ta is suggestive of either reworking of older felsic crust or an active continental margin source while enriched Rb and Ce may be the result of fractional crystallization of magma.

The metasedimentary rocks of the Igarra schist belt are characterized by their geochemical compositions as wacke materials, derived from quartzose sedimentary and felsic igneous provenances in a continental margin environment.

Age data of granitoids indicates two phases of magmatism one in the Paleoproterozoic and the other in the Neoproterozoic. The grey gneiss at 2262 Ma and Dagbala granite gneiss at 2259 Ma represent the first phase of magmatism. The lower intercepts of these two granitoids (555 and 588 Ma respectively) are consistent with lead loss during the Pan African orogenic event. The Igarra granite represents the second phase of magmatism at 599 Ma, and is associated with the Pan African orogenic event.

Given the ages of the grey gneiss and the Dagbala granite gneiss on the one hand and the detrital zircon age distributions of the metasedimentary rocks on the other hand, the former could have been a major source of sedimentary materials to the latter. The basement complex rocks of Nigeria and particularly the metasediments are of low to intermediate metamorphic grade (greenschist to amphibolite facies). It is probable that the Pan African orogenic event represents a major and recorded thermotectonic event that had affected the metasedimentary rocks.

The results of age data for granitoids of the Igarra schist belt are consistent with those of previous age data obtained for different gneissic granitoids associated with the Nigerian basement complex such as OAU Campus granite gneiss (Rahaman and Lancelot, 1984) as well as Jebba (Okonkwo and Ganev, 2012), Kabba (Annor, 1995) and Bode Saadu (Okonkwo and Ganev, 2015) gneisses.

References

Annor, A. E., 1995. Africa Geoscience Review 2, 121-142.

Cox, K.G., Bell, J.D. & Pankhurst, R.J., 1979. George, Allen and Unwin, London.

Cullers, R., 2002. Chemical Geology 191, 305-327.

Floyd, P. A., Winchester, J. A., Park, R. G., 1989. Precambrian Research 45, 203–214.

Hastie, A.R., Kerr, A.C., Pearce, J.A., Mitchell, S.F., 2007. Journal of Petrology 48 (12), 2341–2357

Herron, M.M., 1988. Journal of Sedimentary Research 58, 820-829.

Irvine, T.N. & Baragar, W.R.A. 1971. Canadian Journal of Earth Sciences 8, 523-548.

Maniar, P.D. & Piccoli, P.M. 1989. Geological Society of America Bulletin 101, 635-643.

Marc, D. 1992. Earth Sciences 83, 51-64.

Maynard, J.B., Valloni. R. and Yu. H., 1982. Geological Society of London, Special Publication 10, 551-561.

Okonkwo, C.T. and Ganev, V.Y., 2015. Journal of African Earth Sciences 109, 131-142.

Okonkwo, C.T. and Ganev, V.Y., 2012 International Journal of Geosciences 3, 1065-1073.

Pearce, J.A., Harris, N.B.W. & Tindle, A.G. 1984. Journal of Petrology 25, 956-983.

Peccerillo A, Taylor S.R. 1976. Contribution to Mineralogy & Petrology 58, 63–81.

Rahaman, M.A. and Lancelot, J.R., 1984. Centre Geologique et Geophysique de Montpellier 4, 41.

Roser, B., Korsch, R., 1988. Chemical Geology 67, 119-139.

Detailed Observation of Siderite Iron Formation of the 3.1 Ga Cleaverville Formation, Coastal Pilbara Terrane, Western Australia

Shoichi Kiyokawa [1,2,3], Yushuke Inokuchi[1], Kohei Ishikawa[1]

1. Department of Earth and Planetary Sciences, Kyushu University, Fukuoka, Japan.
2. Center for Advanced Marine Core Research, Kochi University
3. Department of Geology, University of Johannesburg

E-mail− − kiyokawa@geo.kyushu-u.ac.jp

Introduction

The Cleaverville Iron Formation is one of the most important iron formations of the Mesoarchean BIF in the Pilbara greenstone belt. It has been identified within the Gouge Creek Group, which is recognized as the uppermost part of the Pilbara Supergroup (Van Kranendonk et al., 2002, 2004b). It unconformably overlies the Sulphur Springs Group (Hickman & Martin, 2012, Episodes).

The model location of this iron formation is in the coastal greenstone belt, which is tectonically segmented and represents distinct sedimentary successions. We conducted detailed mapping, created a stratigraphic column, and collected fresh samples through scientific drilling in the Cleaverville area (e.g., Miki et al., 2014, Ph.D.).

In this study, we used electron microscopy and chemical analysis to examine the minerals within the Cleaverville Iron Formation, one of the well-known Archean iron formations. Within the coastal Pilbara greenstone belt, there is a well-stratified sedimentary sequence that includes the 3.2 Ga Regal Formation, the Dixon Island Formation (DX Fm), the 3.1 Ga Cleaverville Formation (CL Fm), and the shallow-water Lizard Hills Formation. This region exhibits lower greenschist facies metamorphism and relatively weak deformation and is identified as a volcano-sedimentary sequence in an oceanic island arc setting (Kiyokawa et al., 2006, 2012).

Here, we focus on the stratigraphic variations within the iron formation through detailed observation and description of the CL Fm. High-magnification observations were conducted using optical microscopy, FE-SEM, and TEM.

Results

The CL Fm, which includes a black shale layer transitioning to the BIF layer identified as the "Cleaverville Iron Formation," is well-preserved. It is subdivided into the Black Shale Member and the BIF Member, from bottom to top. The BIF Member preserves the original sedimentary sequence of the BIF.

The Black Chert Member contains 20-10 cm thick organic-rich mud-silt size shale, which includes thin, cross-laminated fine sandstone layers at the base of each bed. The beds are mostly volcaniclastic, with plagioclase fragments increasing towards the top. Thin chert beds (a few cm thick) are observed in the uppermost part of the Black Chert Member.

The BIF Member is subdivided into three submembers: the Siderite-Chert, Magnetite-Chert, and Shale-Chert submembers, from bottom to top. The Siderite-Chert submember consists of bedded greenish shale (GS) and chert/gray mud-laminated beds (CML). In outcrop, the CS beds exhibit a red-white color, while the CML beds form chert-rich iron formations.

The Magnetite-Chert submember comprises GS and chert/magnetite/gray shale alternating beds, where magnetite lamination appears only in the gray mud lamination portions within the CML.

The Shale-Chert submember consists of organic-rich shale and chert-laminated beds. Some laminations display a wavy structure, though no biogenic biomat structures are apparent.

Within the chert beds across the entire member, rounded siderite particles are prominent in the chert/gray mud beds. The siderite particles range from 50-100 μm in diameter, with a central hole and a shell a few microns thick. Siderite appears in three forms: Type 1 includes spherical particles with thin shells, Type 2 features siderite crystallizing around the shell in an angular shape, and Type 3 comprises connected, band-like structures. In the band-like siderite, square siderite crystals are still discernible, some with a small central hole remaining in the middle, all showing signs of diagenetic alteration.

Greenalite (Rasmussen et al., 2013) and berthierine are also identified within the white-pale greenish chert beds.

Discussion

Some portions of this sequence are strongly foliated due to folding along axial plane cleavage. In these early-stage deformed sections, siderite particles appear as sedimentary grains.

We investigated the anoxic and non-sulfidic deep ocean conditions around 3.1 billion years ago, where siderite particles settled on the ocean floor in a muddy silica gel environment. The massive greenish shales may have originated from volcanic tuff, suggesting that widespread volcanic-hydrothermal activity increased during iron-rich sedimentation.

In the future, if the dating accuracy of the Cleaverville BIF in the Pilbara and other regions improves and aligns with the age of the Cleaverville BIF observed in the East Pilbara region, it may indicate the possibility of extensive global hydrothermal or volcanic activities around 3.1 billion years ago, which might be change surface tectonics and ocean water composition.

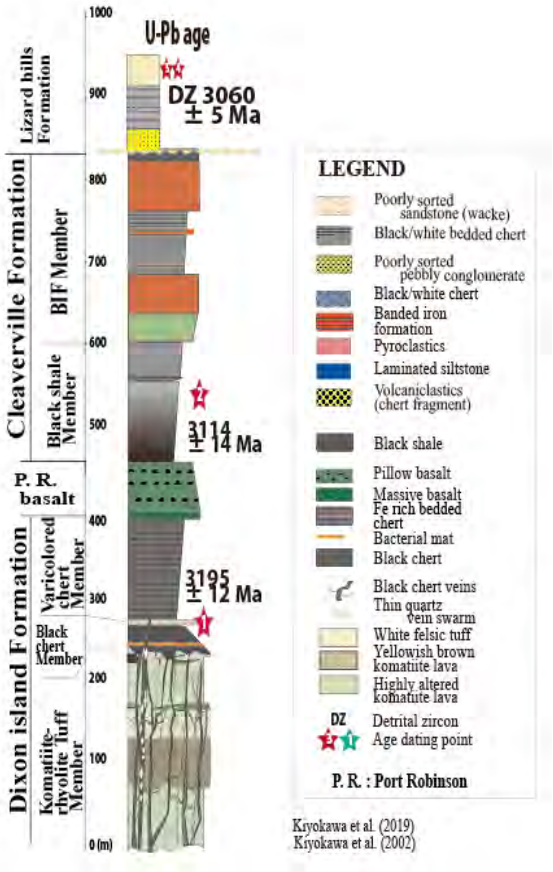

Fig. 3.2 – 3.1Ga Dixon island and Cleaverville Formation, coastal Pilbara terrane, Western Australia.

References

Hickman, A. and Van Kranendonke M.J. (2012) Early Earth evolution: evidence form the 3.5-1.8 Ga geological history of the Pilbara region of Western Australia. Episodo, v. 335, no.1. 283-297.

Kiyokawa, S., et al. (2012) Lateral variations in the lithology and organic chemistry of a black shale sequence on the Mesoarchean seafloor affected by hydrothermal processes: The Dixon Island Formation of the coastal Pilbara Terrane, Western Australia. Island Arc **21**, 118–147.

Kiyokawa S., Ito T., Ikehara M. and Kitajima F., 2006. Middle Archean volcano-hydrothermal sequence: bacterial microfossil- bearing 3.2-Ga Dixon Island Formation, coastal Pilbara terrane, Australia. Geological Society of America Bulletin, vol. **118**, no. 1/2, 3-22.

Rasmussen, B., Meier, D.B., Krapeˇz, B., Muhling, J.R., (2013) Iron silicate microgranules as precursor sediments to 2.5 billion-year-old banded iron formations. Geology **41**, 435–438

Van Kranendonk, M. J., Hickman, A. H., Smithies, R. H., Nelson, D. N. & Pike, G. 2002. Geology and tectonic evolution of the Archaean North Pilbara terrain, Pilbara Craton, Western Australia. Economic Geology, 97, 695–732.

Van Kranendonk, M. J., Collins, W. J., Hickman, A. H. & Pawley, M. J. 2004. Critical tests of vertical vs horizontal tectonic models for the Archaean East

Pilbara Granite-Greenstone Terrane, Pilbara Craton,Western Australia. Precambrian Research, 131,173–211.

THE EASTERN BORDER OF THE SOUTHERN ESPINHAÇO RANGE

Carlos A. Rosière[1], Ricardo Pagung[2]

1. Dep. of Geology, Universidade Federal de Minas Gerais, Belo Horizonte, MG, Brazil
crosiere@gmail.com
2. Dep. of Geology, Universidade Federal de Minas Gerais, Belo Horizonte, MG, Brazil
ripagung@gmail.com

.

1. Introduction

The terranes east of the Southern Espinhaço Range comprise a series of north-south trending ridges, slightly bow-shaped, made up by tectonic slices of the BIF-bearing Serra da Serpentina Group (MDA = 2.0 Ga; Barrote et al., 2017; Rolim et al., 2016), meta-ultramafic rocks and metavolcanic sedimentary units probably of Archean age, and quartzite slivers ascribed to the Serra de São José Group (Rolim et al., 2016), a lateral facies of the São João da Chapada Formation (Lower Espinhaço Sequence - MDA = 1.71 Ga; Chemale et al., 2012). This assembly is juxtaposed with tectonic slices of Archean TTG rocks (3.1 to 2.7 Ga, Rolim, 2016), A-type granites of the Borrachudos Suite (ca. 1.7 Ga, Gomes et al., 2020) and supracrustal sequences of uncertain age (Rhyacian to Statherian).

The scarcity of reliable age constraints in a complex structural scenario associated with the uplift of the crystalline terranes of the Guanhães Inlier as a crustal core complex during the initial stages of the opening of the Espimhaço Basin in the Early Statherian (Pagung de Carvalho, 2024) and the superimposed thin-skinned compressional tectonics developed during the collisional stages of the Brasiliano orogeny, which lasted from the Ediacaran to the Early Cambrian, raise several questions about the age and tectonic evolution of the rocks that form the eastern boundary of the Southern Espinhaço Range. The first concerns the extension of the Paleoproterozoic continental crust (oSao Francisco Paleocontinent) and the Espinhaço Basin, and the second concerns the age and depositional environment of the Serra da Serpentina iron formations.

2. Results

The MDA of the Lower Espinhaço Sequence: The MDA's estimated in this study for the Lower Espinhaço Sequence in the eastern border of the Southern Espinhaço Range and tectonic slivers enclosed in the Borrachudos Granite, range from 1677 ± 16 to 1746 ± 3 Ma in agreement with the depositional dates provided by the geochronological studies of Rolim et al. (2016), Chemale et al. (2012), and with crystallization ages of K-rich alkaline subvolcanic dikes cutting the sedimentary sequences at 1703 ± 12 Ma (Chemale et al., 2012), 1715 ± 2 Ma (Machado et al., 1989) and 1710 ± 12 Ma (Dussin and Dussin, 1995). The age spectra of the detrital zircon populations indicate that the basement (and hinterland) of the Lower Espinhaço Sequence was affected by magmatic activity during four periods: 1-Archean, 2-Siderian, 3- Rhyacian to Late Orosirian, 4-Statherian. The ages of the detrital zircon grains in the Lower Espinhaço Sequence correlate well with magmatic and metamorphic events

The age and depositional environment of the Serra da Serpentina iron formations: Recent fieldwork including mapping associated with geochronological studies of clastic units from the Serra da Serpentina Group of our group Silveira Braga et al. (2015), Rolim et al. (2016), Silveira Braga et al. (2019), Oliveira et al. (2019), indicated that the this unit is truncated in its upper boundary by an erosional unconformity that separates it from the Statherian Serra de São José Group (maximum depositional age = 1666 ± 16 Ma) with the development of a BIF-pebble conglomerate-rich sandstone layer. Rolim et al. (2016) propose an epicontinental sag basin during the Orosirian (youngest detrital zircon U-Pb SHRIMP age = 1990 ± 16 Ma) for the Serra da Serpentina Group exposed at the homonymous area while Pagung et al. (2023) proposed a back-arc basin based on geochemical considerations about the source of the associated clastic sediments (Meloso Fm).

The siliciclastic units of the BIF-bearing successions which occur interleaved with gneissic rocks of the Guanhães Inlier and correlate with the Serra da Serpentina Group provided a detrital age spectrum

that yields a conservative MDA of about 2.18 Ga (Barrote et al., 2017), although these authors recognize a small, but still younger population of 2.10 Ga.

3. Discussion

The results of our current work allow a consistent interpretation of the configuration of the Espinhaço rift during the Early Statherian and the extension of the deposition of clastic sediments on the eastern basin segments beyond the currently established limits, prior to the uplift of the Guanhães Core Complex.

On the other hand, the tectonic environment of the continental basement in the Late Rhyacian is still under discussion and requires further investigation. The few available geochronological data and the detrital contamination of siliciclastic components suggest that the deposition of the Serra da Serpentina iron formation occurred long after the rise in atmospheric oxygen during the Great Oxidation Event (GOE) at 2.4 Ga (Bekker et al., 2004), after or during the final stages of the Rhyacian Minas-Bahia orogen (Bruno et al., 2021), but the tectonic position of the basin is still uncertain. The available ages provided by single detrital zircon grains (1990 ± 16 Ma U-Pb SHRIMP, Rolim et al., 2016) indicate a post-orogenic basin or contemporaneity with volcanic activity during the last collisional events responsible for the assembly of the southeastern and eastern parts of the São Francisco protocraton, the opening of the Sabará foreland basin, and the deposition of volcanoclastic rocks and flysch deposits in the Minas Tectonic Terranes. The MDA for the Sabará Group is usually considered to be about 2.1 Ga (Dopico et al., 2017), and recent data suggest that sedimentation continued until about 2.04 Ga (Dutra et al., 2019) during the collision of the Juiz de Fora arc with the São Francisco margin in the period between 2.10 and 2.00 Ga) with final stabilization of the São Francisco Paleocontinent at ca. 1.94 Ga (Cutts et al., 2018).

In the Southern Espinhaço Range, similar age spectra were obtained by Freimann (2022) from tectonic slices of the Barão do Guaicuí Fm interlayered with quartzites of the Espinhaço SG, where the statistically valid youngest zircon population gives an MDA of 2112 ± 7 Ma (LA-ICPMS), but with the youngest measurement spot at 1980 ± 36 Ma. Detrital zircon grains obtained by Leandro (2022) from quartzite of the Serra Negra Fm overlying the gneissic basement north of the Guanhães Complex yielded a similar youngest date of 1909±37 Ma (LA-ICPMS), which is interpreted as the maximum depositional age.

This complex scenario suggests an alternative compartmentalization of the Paleoproterozoic terranes that make up the Sao Francisco paleocontinent north of the Minas Terranes during the evolution of the Minas Bahia Orogen, causing crustal thinning and subsidence as well the development of hydrothermal vents as the source of iron for the Serpentina BIFs in response to the amalgamation of the Mantiqueira and Juiz de Fora magmatic arcs.

References

Barrote, V. R., Rosiere, C. A., Rolim, V. K., Santos, J. O. S., & McNaughton, N. J. (2017). The proterozoic guanhães banded iron formations, southeastern border of the São Francisco Craton, Brazil: Evidence of detrital contamination. Geologia USP – Serie Cientifica, 17(2), 303–324.

Bekker, A., Holland, H.D., Wang, P-L., Rumble, D., Stein, H.J., Hannah, J.L., Coetzee, L.L., Beukes, N.J., 2004. Dating the rise of atmospheric oxygen. Nature 427, 117–120.

Bruno, H., Heilbron, M., de Morisson Valeriano, C., Strachan, R., Fowler, M., Bersan, S., Moreira, H., Motta, R., Almeida, J., Almeida, R., Carvalho, M., Storey, C., 2021. Evidence for a complex accretionary history preceding the amalgamation of Columbia: The Rhyacian Minas-Bahia Orogen, southern São Francisco Paleocontinent, Brazil. Gondwana Research 92, 149–171.

Chemale, F., Dussin, I. A., Alkmim, F. F., Martins, M. S., Queiroga, G., Armstrong, R., Santos, M. N. (2012). Unravelling a Proterozoic basin history through detrital zircon geochronology: The case of the Espinhaço Supergroup, Minas Gerais, Brazil. Gondwana Research, 22(1), 200–206.

Cutts, K., Lana, C., Alkmim, F., Peres, G.G., 2018. Metamorphic imprints on units of the southern Araçuaí belt, SE Brazil: The history of superimposed Transamazonian and Brasiliano orogenesis. Gondwana Research 58, 211–234.

Dopico, C.I.M., Lana, C., Moreira, H.S., Cassino, L.F., Alkmim, F.F., 2017. U–Pb ages and Hf-isotope data of detrital zircons from the late Neoarchean-Paleoproterozoic Minas Basin, SE Brazil. Precambrian Res 291, 143–161.

Dussin, I.A., Dussin, T.M., 1995. Supergrupo Espinhaço: modelo de evolução geodinâmica. Geonomos. https://doi.org/10.18285/geonomos.v3i1.212

Dutra, L.F., Martins, M., Lana, C., 2019. Sedimentary and U-Pb detrital zircons provenance of the Paleoproterozoic Piracicaba and Sabará groups, Quadrilátero Ferrífero, Southern São Francisco craton, Brazil. Brazilian Journal of Geology 49

Freimann, M. A, 2022 Significado Tectônico das Sequências Metavulcanossedimentares Pré-

Estaterianas da Serra do Espunhaço em Minas Gerais. PhD Thesis. UFMG, 142 pp.

Gomes, S.D., Figueiredo e Silva, R.C., Kemp, A.I.S., Santos, J.O.S., Hagemann, S.G., Lobato, L.M., Rosière, C.A., Novo, T.A., 2020. Zircon U–Pb ages and Hf isotope compositions of Açucena Granite (Borrachudos Suite): Implications for Statherian-Cambrian tectono-magmatic evolution of the southern border of the São Francisco Craton, Brazil. J South Am Earth Sci 100, 102543.

Leandro, U. R.(2021) Gologia da Porção Extremo Norte do Bloco Guanhães,Oógeno Araçuaí (Minas Gerais). MSc Diss. UFMG, 89pp

Machado, N., Schrank, A., Noce, C.M., Gauthier, G., 1996. Ages of detrital zircon from Archean-Paleoproterozoic sequences: Implications for Greenstone Belt setting and evolution of a Transamazonian foreland basin in Quadrilátero Ferrífero, southeast Brazil. Earth Planet Sci Lett 141, 259–276.

Oliveira, L.B.E. da R., Rosière, C.A., Rolim, V.K., Santos, J.O.S., 2019. Novos dados geocronológicos u-pb de zircões detríticos na Serra do Espinhaço Meridional, regiões de Altamira e Ipoema. Revista Geociências UNESP 38, 611–637.

Pagung, R., Rosière, C. A., & Figueiredo e Silva, R. C. (2023). The Serra da Serpentina Group: a back-arc basin related to the Paleoproterozoic Minas-Bahia orogeny? Journal of South American Earth Sciences, 128, 104427.

Rolim, V. K. (2016). As formações ferríferas da região de Conceição do Mato Dentro - MG: posicionamento estratigráfico, evolução tectônica, geocronologia, características geoquímicas e gênese dos minérios [PhD thesis]. Universidade Federal de Minas Gerais.

Rolim, V. K., Rosière, C. A., Santos, J. O. S., & McNaughton, N. J. (2016). The Orosirian-Statherian banded iron formation-bearing sequences of the southern border of the Espinhaço Range, Southeast Brazil. Journal of South American Earth Sciences, 65, 43–66.

Silveira Braga, F.C., Rosière, C.A., Queiroga, G.N., Rolim, V.K., Santos, J.O.S., McNaughton, N.J., 2015. The Statherian itabirite-bearing sequence from the Morro Escuro Ridge, Santa Maria de Itabira, Minas Gerais, Brazil. J South Am Earth Sci 58, 33–53.

Silveira Braga, F.C., Rosière, C.A., Schneider Santos, J.O., Hagemann, S.G., McNaughton, N.J., Valle Salles, P., 2019. The Horto-Baratinha itabirite-hosted iron ore: A basal fragment of the Espinhaço basin in the eastern São Francisco Craton. J South Am Earth Sci 90, 12–33. .

QUATERNARY FOSSILIZED-SPRING CALCAREOUS TUFA OF THE KHARGA OASIS (WESTERN DESERT, EGYPT): SEDIMENTARY RECORDS OF PAST HUMIDITY IN THE EASTERN SAHARA

Fatma A. Mousa[1], Mohamed M. Abu El-Hassan[1], Emad S. Sallam[2]

1. Department of Geology, Faculty of Science, Menoufia University, Egypt
2. Department of Geology, Faculty of Science, Benha University, Benha, Egypt

1. Introduction

Tufa is a variety of carbonate rocks formed as a result of abiotic/microbially precipitation of calcium carbonates from inland alkaline freshwaters including fluvial streams, shallow lakes, lacustrines, palustrines and natural springs at ambient-temperature (Andrews 2006; Sallam 2022). The Kharga Oasis, an erosion-related depression in the south-central part of the Western Desert, appears to be a world-class geosite and a natural laboratory for the study of the fossilized-spring calcareous tufa. The Kharga Depression is made up of a thick-bedded succession of Late Cretaceous-Paleogene age. The depression comprises large, thick accumulations of Quaternary paleospring-deposited tufa being localized at carbonate-dominated areas where karstification process was working actively during periods of increased rainfall and groundwater discharge. Calcareous tufa deposits are widely distributed along the retreated eastern and southern escarpments of the Kharga at the Naqb El-Kharga, Naqb El-Refuf, Naqb Bulaq, Naqb El-Rizeiqat, and Wadi El-Midawara. Tufa deposits in these localities are found at different elevations on the plateau surface, scarp-faces (35m), and along the courses of wadis (5.0m). Lithologically, the investigated tufas are characterized by surficial, soft, semi-friable to solid carbonate crusts, highly porous and vesicular textures, with abundant macrobiological components dominated by *in-situ* encrusted phytoherms and bryophytes, invertebrate snails, algal mats and cyanobacteria. These tufas were most likely deposited by spring-fed fluvial-lacustrine systems, characterized by terraced, vegetated stagnant pools surrounded by arcuate tufa dams and separated by small waterfalls. Photosynthesis and respiration processes by macrophytes, algae and cyanobacteria contributed to CO_2-degassing, facilitated the precipitation of tufa carbonates. Structurally-induced fissures in the older bedrocks provide good paths for groundwater to emerge from shallow karstic aquifers perched above the main Nubian Groundwater Reservoir during Pleistocene pluvial times.

2. Results and discussion

X-ray diffraction analysis of the Kharga tufas showed the predominance of low-Mg calcite. Macroscopic and microscopic investigations revealed the occurrence of both allochthonous and autochthonous components, which consist of clotted, micritic lime-mudstones, peloidal/pisolitic grainstones, phytohermal boundstones, intraclastic rudstones/packstones, laminated crystalline flowstone, and wavy laminated, stromatolitic-like boundstones. Diagenetic features include cementation, recrystallization, micritization and subaerial karstic dissolution. Isotopic signatures from the Kharga tufas displayed negative $\delta^{18}O$ values (average -10.34‰ V-PDB) and negative $\delta^{13}C$ values (average -2.54‰ V-PDB) suggesting precipitation from meteoric environment, probably phreatic under humid conditions with increased rainfall and weathering. The Kharga tufas were dated using uranium-series geochronological method from > 400 ka of plateau tufa to 103 ± 14 ka of scarp tufa and 50.4 ± 0.1 ka of wadi tufa, which correspond to the late marine isotope stage MIS 6 to MIS 5e humid phase determined across N Africa.

Tufas are susceptible sediments to environmental and climatological oscillations (Ford and Pedley 2006; Pedley 2009), therefore, the Kharga tufas can provide critical records of the local/regional terrestrial paleoenvironmental, hydrogeological and paleoclimatic conditions of the eastern Sahara during the recent geological past, the conditions which were fairly humid and, thus, differ from the presently hyperarid climate. Floral pollen-grains incorporated within tufa deposits can also give important signals about paleovegetation and paleoclimate. Additionally, the common occurrence of lithic artifacts encased within the fossil-spring tufas ascertains that the Quaternary pluvial, wet periods of the eastern Sahara were concomitant with human/hominid occupations. Therefore, the great importance of fossilized-spring tufa, as worldwide well-preserved archives helpful for the reconstruction of the past environmental and climatic conditions, encourages us to recommend the establishment of "*Tufa World Geopark*" at the Kharga Oasis which, will promote geotourism, geoconservation, and social-economic sustainable development in this remote oasis in the Sahara.

3. References

Andrews JE (2006) Palaeoclimatic records from stable isotopes in riverine tufas: synthesis and review. Earth-Science Reviews 75: 85–104

Ford TD, Pedley HM (2006) A review of tufa and travertine deposits of the world. Earth-Science Reviews 41:117–175

Pedley HM (2009) Tufas and travertines of the Mediterranean region: a testing ground for freshwater carbonate concepts and developments. Sedimentology 56:221

Sallam ES (2022) Facies and early diagenesis of rainwater-fed paleospring calcareous tufas in the Kurkur Oasis area (southern Egypt). Carbonates and Evaporites 37: 46

THE EVOLUTION OF SINAI AND THE NORTH EASTERN DESERT SEGMENTS THROUGH RIFTING DURING THE INITIATION OF THE PAN-AFRICAN OROGENY

Dawoud, M. ,[*,1] El-Dokouny, H.A.,[2] Mahmoud, A.Sh.,[3] Shebl, A.,[4,5] Abdelkader, M.A.,[6,7] and El-Lithy, M.A.,[8]

1 Geology Department, Faculty of Science, Menoufia University, Egypt
dawoud_99@yahoo.com * Corresponding author
2 Geology Department, Faculty of Science, Menoufia University, Egypt
hanaaabdelnaby4@gmail.com
3 Department of geology, University of Fayoum, Al-Fayoum, Egypt
asm07@fayoum.edu.eg
4,5 Department of Mineralogy and Geology, University of Debrecen, Hungary
Department of Geology, Faculty of Science, Tanta University, Egypt
ali.shebl@science.tanta.edu.eg
6,7 Department of Earth Resource Science, Akita University, Japan
Department of Geology, Faculty of Science, Menoufia University, Egypt
mohammed.ali19924487@gmail.com
8 Geology Department, Faculty of Science, Menoufia University, Egypt
maielleithy24@gmail.com

1. Introduction

In the Arabian Nubian shield, (Fig. 1). the scientists and research articles are mostly talking about the subduction and arc stage: the event, the setting, the outcomes and the related rocks. But what about the pre-arc stage???. The Wilson Cycle postulates the evolution of ocean basins commences with continental breakup (rifting) followed, in sequence, by ocean spreading, subduction initiation, mid-ocean ridge, subduction, and concludes with continent-continent collision. Note that in this simplest form, the Wilson Cycle does not consider the consequences of creation and destruction of back arc basins, or formation, transport and accretion of elongated slivers of pre-existing continent from one continental block to another, Buchs et al., 2013**.** Several questions are arising in this topic, as can be delineated in other orogenies and in comparison, among those 1- when the rifting (or pre-orogenic rifting) in the pan-African orogeny started? What is the event which can be dated (or more or less precisely bracketed and estimated) and considered as the trigger or launching this rifting which in turn define the lower limit of the pan-African orogeny? 2- What are the structural, lithological traces, imprints and outputs of this rift stage? 3- Why the rocks of this stage cannot be inferred or misunderstood or not so obvious or neglected within the Arabian-Nubian shield? 4- How long is the duration of the rifting in the pan-African orogeny and the transitional stage to the widespread subduction stage???

When did the pan-African orogeny start???:

The initial magma that is generated in an orogeny dates and determines the birth of this orogeny. However, there must be time for preliminary tectonics, structural, geomorphological and geological changes until the area becomes fertile and pregnant. A rift is an elongate depression, typically more than 100 km long and tens of kilometers wide, filled with air, water, or rock. It marks a place beneath which the lithosphere has broken in extension, Burke 2011**.** Even before the rift reaches kilometres long or across it becomes trap and place of sedimentation where the accumulation of clastic sediments, organic and chemical precipitates (e.g., evaporites, carbonates, cherts) occurs. As the rift basin widens and deepens two contemporaneous, superimposed or sequential tectono-magmatic events are possible and invoked: 1- the partial melting of the massive and huge rifted crustal blocks due to their friction along the widespread faults, 2- the seepage and eruption of the mantle magma due to the deep faults reaching into the mantle.

2. Results and discussion:

Based on our research results and re-appraisal of published data new ideas concerning the development and evolution of North Eastern Desert and Sinai have been invoked and ascertained. Those data and ideas are related to the preliminary events and the associated rock types that formed the pan-African orogeny and the Arabian-Nubian shield, El-Lithy 2017. The features and evidences can be postulated from geological, lithological, geochemical, isotopes and ages of some relict and inherited zircons, clasts and some exposed intermediate to acidic volcanic and plutonic rock types. Ages from those old staff ranges from 1031 to 740 ma which is clearly older than the first oceanic crust represented in the exposed ophiolites that not older than 750 ma. Of course those age boundaries still need refinement.

Geological, geochemical, isotopes and ages from some exposed rock varieties, clasts and remnant micro-components (relict zircons) refer to pre-oceanic

crust stage in the North Eastern Desert and Sinia. According to the evaluation of the available data and our understanding, deciphering and analyzing the whole events and situation there must be pre-orogenic rifting stage (pre-oceanic crust) pre-date the island arc stage in the Arabian-Nubian shield. That stage resulted in some magmatic activities (pre-orogenic rift-related) that started gradually from the extreme northern tip of the Arabian-Nubian shield (from Sinai; e.g. Um moneiga) into the south (North Eastern Desert, e.g. Um Mongul). According to this scenario zipper rift type is invoked to describe this situation. The magmatic products of this stage are represented by some acidic to intermediate plutonic and volcanic varieties with relatively higher ages compared to their counterparts in the Island arc stage. As those magmatites (and probably some migmatites and metmophites were resulted from (was born by) melting of the pre-existing crust they clearly preserve their chemical signatures with some relict isotopes and ages.

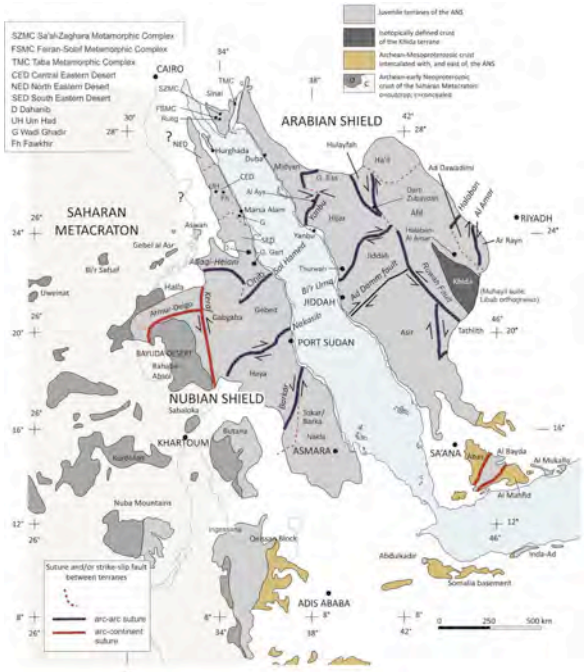

Figure1. Arabian-Nubian shield. After Johnson et al. (2011) and references therein)

References

Buchs, D.M., Bagheri, S., Martin, L., Hermann, J. and Arculus, R., (2013). Paleozoic to Triassic ocean opening and closure preserved in Central Iran: Constraints from the geochemistry of meta-igneous rocks of the Anarak area. *Lithos*, (172-173), pp.267-287. DOI: 10.1016/j.lithos.2013.02.009, Reference: *Lithos* 293.

Burke, K., (2011**).** Plate Tectonics, the Wilson Cycle, and Mantle Plumes: Geodynamics from the Top. *Annu. Rev. Earth Planet. Sci*., 39: 1–29.

El-Lithy,M.A., (2023**).** The Atud diamictite rocks in the Eastern Desert of Egypt: Implications for the paleogeological processes and paleoclimatology. *Unpublished PhD Thesis*, Menoufia University, Egypt. pp. 215.

Johnson PR, Andresen A, Collins AS, Fowler A.R, Fritz H, Ghebreab W, Kusky T, Stern R.J (2011). Late Cryogenian-Ediacaran history of the Arabian-NubianShield: A review of depositional, plutonic, structural, and tectonic events in the closing stages of the northern East African Orogen. *J Afr Earth Sci* 61:167–232

OCCURRENCE AND GEOLOGICAL SETTING OF A NEOPROTEROZOIC IRONSTONE IN THE BUEM STRUCTURAL UNIT (BSU), GHANA

Frank. K. Nyame[1], David Y. Kumah[2], Frank Awuah[3], Daniel Boamah[4],

1. Department of Earth Science, University of Ghana, Legon, Ghana
   fknyame@yahoo.co.uk
2. Ghana Geological Survey Authority, Accra, Ghana
   kumahadinkrahdavid@gmail.com
3. Ghana Geological Survey Authority, Accra, Ghana
   Frank.Awua@ggsa.gov.gh
4. Ghana Geological Survey Authority, Accra, Ghana

1. Introduction

Recent geological mapping by the Ghana Geological Survey Authority within the metacratonic Buem Structural Unit in the southeastern part of Ghana revealed the occurrence of iron-rich rocks within a general succession of basal sandstone, shale, cherty carbonate, chert, ironstone and sandstone.

2. Results

Some of these rocks are, in places, associated with serpentinised mafic/ultramafic bodies. Well preserved and obviously primary iron-rich rocks generally occur as grey to dark grey, massive to well-bedded or banded units traceable for tens of kilometres along strike. Individual bands display variable thickness on the cm scale.

3. Discussion

The

alternating iron and silica rich layers especially present in jaspilitic samples look similar to Rapitan BIF. In general, highly weathered supergene-derived or enriched iron ore overlies the primary material in many areas of outcrop. The occurrence, field relations and general petrographic features, especially the presence in some outcrops of what appears to be "diamictic" features, suggest the ironstone may be closely related to glacial diamictites of the Neoarchean or Sturtian snowball earth events.

Figure1: Banded Iron Formation from the Buem Structural Unit (BSU).

References

Kesse, G. O. (1976). The manganese ore deposits of Ghana. Ghana Geological Survey Bulletin 44, 97pp.

Kleinschrot, D., Klemd, R., Broecker, M., Okrusch, M., Franz, L. & Schmidt, K. (1994). Protores and country rock of the Nsuta manganese deposit (Ghana). Neues Jahrb Miner Abh 168, 67-108.

Layton, W. (1958). The Geology of 1/4o Field sheet No. 32 (Latitude 5o15'–5o30' N. Longitude 0o 30'–0o 45'). Ghana Geological Survey Bulletin No. 24, Accra, Ghana, 66 pp.

Leube, A., Hirdes, W., Mauer, R. & Kesse, G.O. (1990). The Palaeoproterozoic Birimian supergroup of Ghana and some aspects of its associated gold mineralization. Precambrian Research 46, 139–165.

Melcher, F. (1995). Genesis of chemical sediments in Birimian greenstone belts: evidence from gondites and related manganese-bearing rocks from Northern Ghana. Mineralogical Magazine 59, 229–251.

Moreira, C. A. A. A., Borges, M. R., Vieira, G. M. L., Filho, W. M. & Montanheiro, M. A. F. (2012). Geological and geophysical data integration for delimitation of mineralized areas in a supergene manganese deposits Geofisica internacional 53-2, 199-210.

Nyame F. K. (2008). Petrography and geochemistry of intraclastic manganese-carbonates from the ~2.2 Ga Nsuta deposit of Ghana: Significance for manganese sedimentation in the Palaeoproterozoic of West Africa. Journal of African Earth Sciences 50, 133–47.

Nyame, F. K. (1998). Mineralogy, Geochemistry and Genesis of the Nsuta Manganese Deposit, Ghana. Unpublished Ph.D. thesis, Okayama University, Japan.

Nyame, F. K., Katsuo, K. & Yamamoto, M. (1998). Spessartine garnets in a manganiferous carbonate formation from Nsuta, Ghana. Resource Geology 48, 13-22.

Nyame, F.K. (2001). Petrological significance of manganese–carbonate inclusions in spessartine garnet and relation to the stability of spessartine in metamorphosed manganese-rich rocks. Contributions to Mineralogy and Petrology141, 733–746.

Reynolds, J. M. (1995). An introduction to applied and environmental geophysics. John Wiley & sons, New York, 799p.

Roy, S. (1981). Manganese deposits. Academic Press, New York, 458p.

MINERALOGICAL AND GEOCHEMICAL SIGNATURE OF GOLD MINERALIZATION AT ESAASE MINE, AKROMA GOLD, NORTHEASTERN AXIM-KONONGO (ASHANTI) BELT, GHANA: IMPLICATIONS FOR MINING AND ENVIRONMENTAL MANAGEMENT

Kwabina Ibrahim[1], Frank K. Nyame[2], Alfred A. Yankson[3]

1. Department of Earth Science, University of Ghana, Legon, Ghana
   Kwabina.ibrahim@gmail.com
2. Department of Earth Science, University of Ghana, Legon, Ghana
   fknyame@yahoo.co.uk
3. Department of Physics, University of Ghana, Legon, Ghana
   AYankson@ug.edu.gh

1. Introduction

Integrated petrographic, Scan electron Microprobe, and geochemical investigations of ore and host rock samples from the Esaase mine, Akroma Gold, reveal valuable insights into gold mineralization.

2. Results

Scan electron Microprobe analysis confirms gold occurrence in fractures, inclusions, and occlusions within pyrite, with potential sub-microscopic gold grains in matrix quartz, carbonate, and mica.

Geochemical data show:
- Gold correlation with pyrite and sphalerite
- Arsenopyrite (FeAsS) and galena (PbS) rarity or absence, minimizing environmental concerns
- Low concentrations of deleterious elements (As, Pb)

3. Discussion

In general, rarity or absence of arsenopyrite (FeAsS) and galena (PbS) in many samples of both ore and host rocks investigated that could potentially contribute deleterious elements (e.g. arsenic and lead) suggests that the Akoase mineralisation may be mined and/or processed without much introduction of these potentially harmful elements into the surrounding environmental compartments.

Figure1: Photograph of the rock specimen, showing pyrites.

References

Abouchami, W., Boher, M., Michard, A., Albarede, F., 1990. A major 2.1 Ga event of mantle magmatism in West Africa: an early stage of crustal accretion.J. Geophys. Res. 95, 17605-17629.

Anum, S., Sakyi P. A., Su, B. X., Nude, P. M., Nyame, F., Asiedu D., Kwayisi, D., 2015. Geochemistry and geochronology of granitoids in the Kibi-Asamankese area of the Kibi-Winneba volcanic belt, southern Ghana. J. Afr. Earth Sci. 102, 166–179.

Barth, T.F.W., 1948. Oxygen in rocks: a basis for petrographic calculation. J. Geol. 56, 50-60.

Bartley, J.M., 1986. Evaluation of REE mobility in low-grade metabasalts using massbalance calculations. Nor. Geol. Tidsskr. 66, 145-152.

Beziat, D., Bourges, F., Debat, P., Lompo, M., Martin, F., Tollon, F., 2000. A Paleoproterozoic ultramafic-mafic assemblage and associated volcanic rocks of the Boromo greenstone belt: fractionates originating from island-arc volcanic activity in the West African craton. Precambrian Res. 101, 25-47.

Cann, J.R., 1970. Rb, Sr, Y, Zr and Nb in some ocean-floor basaltic rocks. Earth Planet. Sci. Lett. 19, 7-11.

Condie, K.C., 2005. High field strength element ratios in Archean basalts: a window to evolving sources of mantle plumes? Lithos 79, 491-504.

Davis, D.W., Hirdes, W., Schaltegger, U., Nunoo, E.A., 1994. U–Pb age constraints on deposition and provenance of Birimian and gold-bearing Tarkwaian sediments in Ghana, West Africa. Precambrian Research 67, 89–197

TEXTURAL AND ISOTOPIC ($\delta^{13}C$ AND $\delta^{34}S$) RECORDS FROM CARBONACEOUS SEDIMENTARY ROCKS FROM THE PALEOPROTEROZOIC BIRIMIAN OF NW GHANA, WEST AFRICA: IMPLICATION ON POTENTIAL GOLD SOURCE

Samuel Nunoo[1,2], Axel Hofmann[2], and Mike Butler[3]

1. Department of Earth Science, University of Ghana, Legon-Accra, Ghana
   snunoo@ug.edu.gh
2. Department of Geology, University of Johannesburg, South Africa
   ahofmann@uj.ac.za
3. National Research Foundation, iThemba Labs, Johannesburg, South Africa
   butler@tlabs.ac.za

1. Introduction

Carbonaceous sedimentary rocks are common in the Paleoproterozoic Birimian of Ghana, and mostly host gold mineralization that occurs as free milling type in quartz-veins or as a refractory type within quartz vein-associated sulphide (Oberthur et al., 1997). The association of organic and sulphidic-rich rocks with gold occurrences is considered a prominent metallogenic source (e.g. Tomkins, 2013; Hu et al., 2016). Shale (Fig. 1a) and greywacke (Fig. 1b) from the sedimentary succession of the Julie belt in NW Ghana have been examined petrographically at the University of Johannesburg (UJ). Isotope data (carbon-$\delta^{13}C$ and sulphur-$\delta^{34}S$) was collected on samples at the NRF-Ithemba Labs (South Africa) using the Flash HT Plus elemental analyser coupled to a Delta V Advantage isotope ratio mass spectrometer by a ConFloIV interface. Gold content in bulk rocks and sulphides was measured using an ICP-MS facility at BVM laboratory (Vancouver, Canada) and a CAMECA SX100 electron probe microanalyser (EPMA) at UJ respectively.

2. Results

Samples show a moderate to dark grey colour due to variable content of organic matter (OM). Greywacke contains fine-grained pyrite (Fig. 1b) with distorted colloform features (Fig. 1c) of irregular concentric laminae and layer of pyrite. Greywacke is weakly deformed relative to the shale samples. Sheared shale is marked by milky to translucent Qz-Cb ± K-Fsp veins associated with arsenopyrite (Fig. 1a). SEM-EDS analyses indicate that sulphides (Fig. 1d) are commonly arsenopyrite and pyrite with minor chalcopyrite. Sulphides occur as disseminations but are mostly restricted to cleavage planes rich in carbonaceous matter (Fig. 1d), iron oxides and chlorite. Arsenopyrite dominates with needle-like shapes parallel to foliation, and occurs as intergrowths or as overgrowths largely with pyrite. The shales and greywackes have $\delta^{13}C$ values in the range of -23.0 to -14.0 ‰ and -27.0 to -30.0 ‰ (Table 1) respectively. Sulphur-$\delta^{34}S$ values (Table 1) from the shales and greywackes show respective range of -8.0 to -22.0 ‰ and -0.8 to +5.0 ‰. Bulk rock ICP-MS gold analysis of samples reveal traces of gold in greywacke (1.8 to 4 ppb) and sheared shale (1.3 to 1482 ppb). EPMA of sulphide from mineralized sheared shales recorded assay values of 4 –176 ppm.

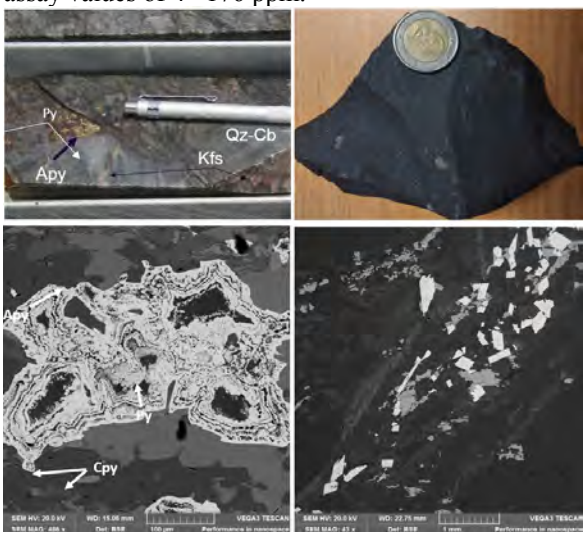

Figure 1. (a) Sheared carbonaceous shale characterized by quartz (Qz)- carbonate (Cb)-sulphide ± potassium feldspar (K-Fsp) vein. (b) Hand sample of organic rich-greywacke containing fine-grained pyrite. (c) Distorted colloform feature marked by µm-scale irregular concentric laminae and layer of pyrite. (d) Sheared graphitic shale contains aggregates of pyrite (Py) and arsenopyrite (Apy) along foliation plane

Table 1: Carbon and sulphur isotope composition of shales and greywackes from the Julie belt, NW Ghana

Samples	Rock type	$\delta^{13}C$ (‰)	$\delta^{34}S$ (‰)

C1-1	Shale	-18.0	-8.0
C1-2	Shale	-21.0	–
C1-3	Shale	-21.0	–
C2-3	Shale	–	-9.0
A1	Shale	-20.0	-13.0
A7	Shale	–	-22.0
A9	Shale	-23.0	-18.0
K7-2	Shale	-14.0	–
DAN1	Greywacke	-28.0	+4.0
SDK	Greywacke	-30.0	-0.8
SDK 3	Greywacke	-27.0	+5.0
SDK 4	Greywacke	-28.0	+2.0

3. Discussion

In greywackes, the presence of colloform pyrite depicts a diagenetic growth processes within a sedimentary environment; the pyrite growth developed largely via biogenic activity, and other likely growth mechanisms of pseudomorphic replacement and inorganic precipitation during formation (e.g., Gao et al., 2016). The distorted colloform textures as ellipsoidal form are consequences of subsequent deformation and/or metamorphic events. Conversely, in sheared shales, the remarkably well-formed textural features of arsenopyrite and subordinate pyrite restricted to CM-rich foliation planes suggest syn-kinematic and syn- to late metamorphic crystallisation of these sulphides; and are part of the secondary hydrothermal activity due to association with quartz-carbonate veins.

The carbonaceous and sulphidic-rich shale and greywacke are possible sources for Birimian metasedimentary-hosted Au in NW Ghana gold deposits; and that microbial activities likely facilitated the formation of precursor sulphides that incorporated Au; which was later transported via suitable structural conduits by probable complexes of Au-S and/or organic-ligands; and became trapped/deposited into recrystallized euhedral sulphides largely of arsenopyrite and pyrite, and less commonly chalcopyrite.

The $\delta^{13}C$ and $\delta^{34}S$ isotope characteristics of sheared shales and organic-rich greywackes indicate that biological processes or sources played a role during the sedimentary derivation of these rocks and subsequent gold mineralization. And that the CM present in these rocks may have played multiple roles; as a major control on pyrite formation (e.g., Berner, 1984; Falconer et al., 2006), as an electron donor in gold precipitation (e.g. Craw et al., 2015); as organic ligands in Au transport (e.g. Williams-Jones and Migdisov, 2007); as a reductant that reacts with Au-bisulfide to cause direct deposition of gold (Hayashi and Ohmoto, 1991); and as lubricant that may aid in the formation of shear zones (e.g. Upton and Craw, 2014).

References

Allibone, A., McCuaig, C., Harris, D., Etheridge, M.A., Munroe, S., and Byrne, D., 2002. Structural controls on gold mineralization at the Ashanti gold deposit, Obuasi, Ghana. Society of Economic Geologists, Special Publication 9, 65 – 93.

Berner, R.A., 1984. Sedimentary pyrite formation: An update*. Geochimica et Cosmochimica Acta 48 (4), 605 – 615.

Craw, D., Mortensen, J., MacKenzie, D., Pitcairn, I., 2015. Contrasting geochemistry of orogenic gold deposits in Yukon, Canada and Otago, New Zealand. Geochemistry: Exploration Environmental and Analytical 15, 150-166.

Falconer, D.M., Craw, D., Youngson, J.H., and Faure, K., 2006. Gold and sulphide minerals in Tertiary quartz pebble conglomerate gold placers, Southland, New Zealand. Ore Geology Reviews 28(4), 525 –545.

Gao, S., Huang, F., Wang, Y., Gao, W., 2016. A Review of Research Progress in the Genesis of Colloform Pyrite and Its Environmental Indications. Acta Geologica Sinica (English Edition). 90, No. 4, 1353 –1369.

Hayashi, K., and Ohmoto, H., 1991. Solubility of gold in NaCl and H2S bearing aqueous solutions at 250-350°C. Geochimica et Cosmochimica Acta 55, 2111 – 2126.

Hu, S.-Y., Evans, K., Fisher, L., Rempel, K., Craw, D., Evans, N.J., Cumberland, S., Robert, A., Grice, K., 2016. Associations between sulfides, carbonaceous material, gold and other trace elements in polyframboids: Implications for the source of orogenic gold deposits, Otago Schist, New Zealand. Geochimica et Cosmochimica Acta 180, 197 – 213.

Oberthür, T., Weiser, T., Amanor, J.A., Chryssoulis, S.L., 1997. Mineralogical sitting and distribution of gold in quartz veins and sulfide ores of the Ashanti mine and other deposits in the Ashanti belt of Ghana: genetic implications. Mineralium Deposita 32, 2–15.

Tomkins, A.G., 2013. A biogeochemical influence on the secular distribution of orogenic gold: Economic Geology and the Bulletin of the Society of Economic Geologists, 108, 193–197.

Upton, P., Craw, D., 2014. Modelling of structural and lithological controls on mobility of fluids and gold in orogenic belts, New Zealand. Geological Society London, Special Publication 402, 231 –253.

Williams-Jones, A., Migdisov, A., 2007. The solubility of gold in crude oil: implications for ore genesis, Proceedings of the 9 th Biennial SGA Meeting, Dublin. Millpress, 765 –768.

Reconstruction of the stratigraphic and structural development history of the Paleoproterozoic Birimian Belt in the Cape Three Points area, southwestern Ghana

Satoshi Yoshimaru[1], Shoichi Kiyokawa[1], Takashi Ito[2], Kenji Horie[3], Mami Takehara[3], Kwabina Ibrahim[4], George M. Tetteh[4], and Frank K. Nyame[5]

1. Department of Earth and Planetary Sciences, Kyushu University, Fukuoka, Japan (Yoshimaru.satoshi.536@s.kyushu-u.ac.jp)
2. Ibaraki University, Mito, Japan.
3. National Institute of Polar Research, Tokyo, Japan.
4. University of Ghana, Legon, Ghana.
5. University of Mines and Technology, Tarkwa, Ghana.

1. Introduction

The Leo-Man Shield of the West African Craton (WAC, Fig.1) is a crustal massif in the sub-Saharan region of West Africa, and several greenstone belts called the Birimian, which were formed about 2.3 to 2 Ga, are distributed in its eastern part of the shield (Milesi et al., 1992). It is not clearly understood that the tectonic development of oceanic island arc crusts (until about 2.2 Ga) that are assumed to be a protoliths of the Birimian greenstone belts (Grenholm et al., 2019). In this study, we focus on the southern Ashanti Belt in Ghana, which only has areas exposing the sedimentary sequences of the Birimian along the coastline in the WAC. The continuous outcrop is expected to provide records of formation process of this Birimian oceanic island arc crust. Especially in the Cape Three Points area, a well-continuous volcanic-volcaniclastic stratigraphy is exposed. The depositional age of them was constrained to before 2172 Ma by zircon age of granitic intrusions (Hirdes et al., 1992). The objective of this study is to clarify the stratigraphy, structure, and age of the volcanic rocks in order to reconstruct the tectonic evolution and stratigraphic history of the area.

2. Stratigraphy

Field survey revealed a continuous lithologic succession of about 8000 m in total structural thickness from ultramafic complex in the western part to volcaniclastic metasedimentary rocks in the eastern part. Those rocks strike NE-SW trend with some local variation, and eastward dipping and younging. The eastern flank of the study area is margined by later granitoid. At the western flank of the ultramafic complex is bounded from the western granitoid pluton with a small amphibolite deformation zone. The eastern volcaniclastic sequence is structurally overlying the ultramafic complex. There are well-preserved stratigraphic units that are mainly composed of basalt and andesitic volcaniclastic turbidite deposits and pyroclastic deposits. The lower unit consisting with

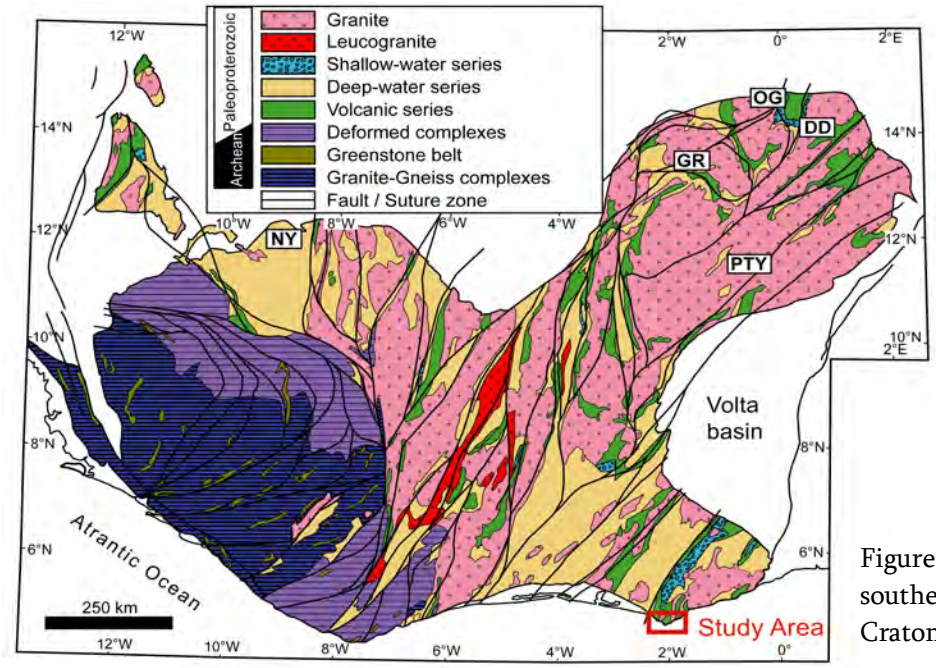

Figure 1. Geological map of southern West Africa Craton (after Milesi et al.,

fine-grained turbidite represents constant input resulted in the rhythmical volcaniclastic turbidity sequence. On the other hand, the upper sequence consisting with coarser and thicker volcaniclastic deposits and lava deposit, which represents larger volcanic event deposits intercalated within the constant sedimentation condition. At the top of the sequence, the volcaniclastic deposits changed to dacitic composition from basaltic-andesitic deposits of the lower and upper parts. These volcaniclastic and volcanic rocks occurred in the area were volcanic-arc basalt type chemical compositions in the discrimination method by Pearce (1973).

3. Geochronology (U-Pb zircon)

The uppermost dacitic tuff was dated and the mean 2172±6.1 Ma (SHRIMP, n=35, MSWD=1.07). Mean age of a porphyry dike intruded into the volcaniclastic beds in the upper middle part of the sequence was 2265±4.6 Ma (SHRIMP, n=48, MSWD=0.95). Leucogabbro occurred in eastern flank of the ultramafic complex was 2282.28±0.57 Ma (CA-ID-TIMS, n=3).

4. Discussion

Geology of the study area is estimated to have been formed by long-term continuous volcanic material supply of basaltic, andesitic and dacitic volcanic sediments into sedimentary basins around the island arc volcanoes. That basin is underlain by the ultramafic complex which could be architected at 2.28 Ga as a basin basement. Overlying basaltic and andesitic volcanic sediments were deposited on the basement before 2.26 Ga. They are covered by the dacitic volcaniclastics of 2.17 Ga at the top of the sequence. It likely has a stratigraphic hiatus of about 90 million years between them. The 2.17 Ga dacitic volcanism was synchronous with the surrounding large granitoids (Hirdes et al., 1992), which could be a timing of the magmatic evolution of the region. So, this should be distinguished from the early basaltic and andesitic volcanism in the Ashanti belt, for the better classification of the volcanic stratigraphy.

Geochronological constraints suggest that island-arc igneous activities of the Ashanti belt have started around 2.28-2.26 Ga, which infers the subduction deriving the magmatism in the Ashanti belt was initiated before that.

References

Milési, J. P., Ledru, P., Feybesse, J. L., Dommanget, A., & Marcoux, E. (1992). Early Proterozoic ore deposits and tectonics of the Birimian orogenic belt, West Africa. *Precambrian Research*, *58*(1-4), 305-344.

Grenholm, M., Jessell, M., & Thébaud, N. (2019). A geodynamic model for the Paleoproterozoic (ca. 2.27–1.96 Ga) Birimian Orogen of the southern West African Craton–Insights into an evolving accretionary-collisional orogenic system. *Earth-science reviews*, *192*, 138-193.

Hirdes, W., Davis, D. W., & Eisenlohr, B. N. (1992). Reassessment of Proterozoic granitoid ages in Ghana on the basis of U/Pb zircon and monazite dating. *Precambrian Research*, *56*(1-2), 89-96.

Pearce, J. A., & Cann, J. R. (1973). Tectonic setting of basic volcanic rocks determined using trace element analyses. *Earth and planetary science letters*, *19*(2), 290-300.

THE GEOLOGY OF GOLD MINERALIZATION IN THE NANGODI GREENSTONE BELT, NE GHANA

Kwame Fynn[1], Axel Hofmann[2] and Samuel Nunoo[3]

1. Department of Geology, University of Johannesburg, Johannesburg, South Africa kfynn@uj.ac.za
2. Department of Geology, University of Johannesburg, Johannesburg, South Africa ahofmann@uj.ac.za
3. Department of Earth Science, University of Ghana, Legon, Accra, Ghana kingnunoo2000@gmail.com

1. Introduction

The Birimian of the West African Craton comprises a Palaeoproterozoic granitoid-greenstone terrain. Among the greenstone belts is the NE-SW trending Bole-Nangodi belt located in the northern part of Ghana (Leube et al., 2009; Block et al., 2016). It consists of volcanic and volcaniclastic rocks (basalt to rhyolite) and immature sedimentary rocks (greywacke, shale), and is flanked on both sides by extensive granitoid complexes (Attoh, 1982; de Kock et al., 2012; Block et al., 2016). These rocks have been affected by the 2.1 Ga Eburnean orogeny, which deformed and metamorphosed the rocks under greenschist facies conditions, accompanied by gold mineralization (Abouchami et al., 1990; Feybesse et al., 2006). Until the recent gold deposit discovery by Cardinal Resources (Namdini Gold Project) in the Nangodi belt (Tomlinson et al., 2020), very little attention had been given to the rocks in the belt and the associated gold mineralization. This study presents U-Pb zircon ages, (ore) petrographic observations, and whole rock major and trace element data, from outcrop and drill core samples (including drill cores from the Namdini Gold Project).

2. Results

Rock types identified in the area include metavolcanic rocks of basaltic to andesitic origin that may be calc-alkaline or tholeiitic, muscovite granite, alkali feldspar (Bongo) granite and organic-rich shales. These rocks are generally deformed and characterized by intense alteration associated with CO_2-rich hydrothermal fluids, and sulphide mineralization that hosts gold. Hydrothermal gold mineralization is associated with disseminated sulphides that occur with quartz-carbonate veins and are usually restricted to high-strain zones in the metavolcanic rock. Two types of sulphide mineralization in the area are; Type I – pyrite-arsenopyrite-dominated, and Type II – pyrite-dominated. U-Pb data yielded ages of 2160 ± 4 Ma for the metavolcanics, 2119 ± 5 Ma for the muscovite granite and 2100 ± 9 for the alkali feldspar granite

3. Discussion

Geochemical characteristics of the rocks in the area suggest arc-related volcanism and plutonism accompanied by sedimentation in inter-arc basins. However, the rocks have been deformed and metamorphosed under greenschist facies conditions resulting in high-strain domains characterized by quartz-carbonate veins and associated sulphide mineralization. Deformed veins, foliation-parallel orientation of sulphides and pressure shadows suggest syn-tectonic precipitation of the sulphides. Compositional zoning in the sulphides implies changes in the chemistry of ore-forming fluids resulting in two main stages of ore deposition (stage I – earlier pyrite-arsenopyrite deposition; stage II – late-stage pyrite deposition). The gold is hosted as solid solutions mainly in arsenian pyrite and arsenopyrite. The metavolcanic rocks were deposited at ca. 2160 Ma and were intruded by muscovite granite and alkali feldspar granite at ca. 2119 Ma and 2100 Ma with gold mineralization occurring in the time interval between the emplacements of the granites.

References

Abouchami, W., Boher, M., Michard, A. and Albarede, F. 1990. A major 2.1 Ga event of mafic magmatism in west Africa: An Early stage of crustal accretion. Journal of Geophysical Research: Solid Earth, 95, 17605–17629.

Attoh, K. 1982. Structure, gravity models and stratigraphy of an early Proterozoic volcanic—sedimentary belt in northeastern Ghana. Precambrian Research, 18, 275–290.

Block, S., Jessell, M., Aillères, L., Baratoux, L., Bruguier, O., Zeh, A., Bosch, D., Caby, R. and Mensah, E. 2016.

Lower crust exhumation during Paleoproterozoic (Eburnean) orogeny, NW Ghana, West African Craton: Interplay of coeval contractional deformation and extensional gravitational collapse. Precambrian Research, 274, 82–109.

de Kock, G.S., Théveniaut, H., Botha, P.M.W. and Gyapong, W. 2012. Timing the structural events in the Palaeoproterozoic Bolé–Nangodi belt terrane and adjacent Maluwe basin, West African craton, in central-west Ghana. Journal of African Earth Sciences, 65, 1–24

Feybesse, J.-L., Billa, M., Guerrot, C., Duguey, E., Lescuyer, J.-L., Milesi, J.-P. and Bouchot, V. 2006. The Paleoproterozoic Ghanaian province: Geodynamic model and ore controls, including regional stress modeling. Precambrian Research, 149, 149–196.

Leube, A., Hirdes, W., Mauer, R. and Kesse, G.O. 1990. The early Proterozoic Birimian Supergroup of Ghana and some aspects of its associated gold mineralization. Precambrian Research, 46, 139–165.

Tomlinson, K., Abbott, P., Opoku-Boamah, E., Owusu-Ansah, E., Affi, S., Bray, R. and Taylor, E. 2020. Namdini Gold Deposit, Upper East Region, Ghana - One of the Largest West African Gold Discovery in a Decade. Cardinal Resources Limited.

Accessing the Ediacaran-Cambrian boundary in SW Baltica based on SHRIMP and CA-ID-TIMS zircon U-Pb dates

Ion Francovschi[1,5], Maria Ovtcharova[2], Mami Takehara[3], Kevin Chamberlain[4], Joseph Feldman-Peterson[5], Andrey Bekker[5,6]

1. Moldova State University, Institute of Geology and Sesimology, Moldova frankovski.ww@gmail.com
2. Department of Earth Sciences, University of Geneva, Switzerland
3. National Institute of Polar Research, Tokyo, Japan
4. Department of Geology and Geophysics, University of Wyoming, Laramie, USA
5. Department of Earth and Planetary Sciences University of California, Riverside, CA 92521, USA
6. Department of Geology, University of Johannesburg, Auckland Park, Johannesburg 2006, South Africa

1. Introduction

In recent years, using the youngest detrital zircon dates for sedimentary deposits, generated with the LA-ICP-MS technique, has become a common method for constraining depositional ages. Researchers often use the Maximum Depositional Age (MDA) as a proxy for a True Depositional Age (TDA). However, it has been shown that Pb loss from zircon can significantly affect LA-ICP-MS U–Pb zircon dates (Sharman and Malkowski, 2024), potentially resulting in individual zircon U-Pb dates being younger than their crystallization ages (Sharman and Malkowski, 2020).

In the Moldova-Podillya basin in southwestern Baltica, Paszkowski et al. (2021) conducted U-Pb LA-ICP-MS analyses on zircons from sandstones of the lower Kanyliv Group, obtaining MDA ages of 529 ± 10 Ma, 532 ± 6 Ma, 531 ± 8 Ma, and 523 ± 5 Ma, which are inconsistent with known biostratigraphic age constraints, indicating the late Ediacaran age (e.g., Ivantsov et al., 2015). Previously, the boundary between the late Ediacaran (Kanyliv Group) and early Cambrian (Baltic Group) was defined by the first appearance of the *Phycodes* (=*Trichophycus*) *pedum* ichnofossil zone (e.g., Ivantsov et al., 2015). However, the obtained ages suggest that this boundary should be placed below the Kanyliv Group, at the contact with the Mohyliv-Podilsky Group.

To address this discrepancy between geochronologic and biostratigraphic data with the view of the recently highlighted concern over undetected Pb loss in LA-ICP-MS analyses affecting the dates, zircon treatment by chemical abrasion (CA) and analysis using isotope dilution–thermal ionization mass spectrometry (ID-TIMS) is required. We sampled sandstones from the lowermost part of the Pylypy Beds, Danylivka Formation, lower Kanyliv Group, in the northern Moldova-Podillya basin, near the village of Naslavcea, Ocnita county, Moldova. The zircons were dated using the SHRIMP U-Pb method, followed by U-Pb CA-ID-TIMS, to determine whether the Kanyliv Group belongs to the late Ediacaran or early Cambrian.

2. Results

Following standard zircon separation procedures, 200 detrital zircons were dated using the U-Pb SHRIMP method, of which 115 were concordant. Using the Maximum Likelihood Age (MLA) method (Vermeesch, 2021), the MDA was determined to be 530 ± 10 Ma. After chemical treatment and subsequent ID-TIMS dating, the same zircons that defined the MDA yielded an age of 553.20 ± 0.25 Ma, consistent with the biostratigraphic constraints.

3. Discussion

The Maximum Depositional Age (MDA) obtained with the SHRIMP U-Pb dating of detrital zircons from the Pylypy Beds, Danylivka Formation, lower Kanyliv Group in the northern Moldova-Podillya basin yielded an age of 530 ± 10 Ma, which is younger than the revised Ediacaran-Cambrian boundary age of 538.8 ± 0.2 Ma (Linnemann et al., 2019). Such result would necessitate reconsidering the Ediacaran-Cambrian boundary placement in southwestern Baltica. However, CA-ID-TIMS dating of the same youngest zircons provided a markedly older age of 553.20 ± 0.25 Ma, emphasizing the importance of using CA-ID-TIMS for high-precision chronostratigraphic studies, as Pb loss can cause an apparently younger date than the depositional age of sediments.

References

Ivantsov, A.Yu., Gritsenko, V.P., Paliy, V.M., Velikanov, V.A., Konstantinenko, L.I., Menasova, A.Sh., Fedonkin, M.A., Zakrevskaya, M.A., Serezhnikova, E.A. (2015). Upper Vendian macrofossils of Eastern Europe. Middle Dniester area and Volhynia. Moscow, PIN RAS. 1–144.

Linnemann, U., Ovtcharova, M., Schaltegger, U., G¨artner, A., Hautmann, M., Geyer, G., Vickers-Rich, P., Rich, T., Plessen, B., Hofmann, M., Zieger, J., Krause, R. (2019). New high-resolution age data from the Ediacaran-Cambrian boundary indicate rapid, ecologically driven onset of the Cambrian explosion. *Terra Nova* **31**, 49–58.

Paszkowski, M., Budzyń, B., Mazur, S., Sláma, J., Środoń, J., Millar, I.L., Shumlyanskyy, L. (2021). Detrital zircon U-Pb and Hf constraints on provenance and timing of deposition of the Mesoproterozoic to Cambrian sedimentary cover of the East European Craton, part II: Ukraine. Precambrian Research 362, 106282.

Sharman, G.R., Malkowski, M.A. (2020). Needles in a haystack: Detrital zircon UePb ages and the maximum depositional age of modern global sediment. *Earth-Science Reviews* **203**, 103109.

Sharman, G.R., Malkowski, M.A. (2024). Modeling apparent Pb loss in zircon U–Pb geochronology. *Geochronology* **6**, 37–51.

Vermeesch, P. (2021). Maximum depositional age estimation revisited. *Geoscience Frontiers* **12**, 843–850.

TRACING OXIDATIVE U CYCLE WITH PB ISOTOPES IN MARINE CARBONATES

Andrey Bekker[1, 2], Robert Bolhar[3]

1. Department of Earth and Planetary Sciences, University of California, Riverside, CA 92521, USA andreyb@ucr.edu
2. Department of Geology, University of Johannesburg, P.O. Box 524, Auckland Park, Johannesburg 2006, South Africa
3. School of Geosciences, University of Witwatersrand, Braamfontein, 2001 South Africa robert.bolhar@wits.ac.za

1. Introduction

The Great Oxidation Episode (GOE) at 2.43-2.1 Ga irreversibly changed biogeochemical cycling on Earth's low-oxygen surface towards conditions controlled by free atmospheric oxygen. Before that redox cycling was only locally expressed near "oases" with high primary biological productivity. Uranium as a redox-sensitive element is insoluble under anoxic surface conditions, like Th, but decouples from Th under oxic surface conditions, resulting in its high concentration in modern oxic oceans ($3*10^{-9}$ g U vs. $0.4*10^{-15}$ g Th) and corresponding long seawater residence time. It is removed in anoxic settings and thus strongly enriched in organic-rich shales. Compilation of U concentration data for Precambrian and Phanerozoic black shales (Partin et al., 2013) revealed that the pre-GOE shales are not strongly enriched in U above the average upper continental crust (UCC; Rudnick and Gao, 2014) level, consistent with largely anoxic surface conditions during their deposition. However, concentration data cannot unequivocally resolve whether U was still soluble at low concentrations in seawater at the time of deposition. A long-term record, utilizing a highly sensitive redox proxy, is therefore required to address this question. Modern, pure carbonates have ppm-level concentrations of U, derived from seawater, whereas their Th contents are very low. The Precambrian carbonate record is therefore well suited to explore when U and Th became decoupled in seawater due to oxidative surface processes.

2. Results

U-Pb and Pb-Pb isotope dated, shallow-marine, sedimentary carbonates may bear on U decoupling from Th in the pre-GOE surface environments. A compilation (~80 datasets) of U-Pb and Pb-Pb isotope data from literature for sedimentary carbonates with dates close to their depositional ages, ranging between 3.1 Ga and 50 Ma, indicates that their U-Pb and Pb-Pb isotope systems were not affected by post-depositional alteration and remained closed since carbonate deposition. The isotope data has been screened for outliers and was used to calculate time-averaged kappa (Th/U) values with propagated uncertainties to constrain whether U and Th were coupled or decoupled in seawater from which these carbonates precipitated. While there are few pre- and syn-GOE, and ca. 1.9 Ga literature datasets with near to or even above the average upper continental crust (UCC) kappa values ($\kappa \approx 4.0$; Rudnick and Gao, 2014), the majority of the dataset yield values <1.4, well below the UCC kappa value regardless of their depositional age.

2. Discussion

These data indicate that U was decoupled from Th in the early Earth oceans since at least ca. 3.0 Gyr ago, and must have been soluble at low concentrations under largely anoxic terrestrial and shallow-marine conditions during the Archean. It requires that some U was oxidized on land, transported in rivers as dissolved U^{6+}, and delivered to and deposited with carbonates on shallow-marine carbonate platforms, and with organic matter in anoxic deeper marine settings. There is a significant change in the average Th/U during the GOE towards lower values, indicating growth in the seawater U reservoir under oxygenated atmospheric and shallow-marine conditions. Finally, the second ingrowth in seawater U reservoir corresponds to the Neoproterozoic Oxygenation Event in the late Neoproterozoic.

References

Partin et al., 2013, EPSL 369-370, 284-293.
Rudnick and Gao, Treatise of Geochemistry, 2014.

NITROGEN CYCLING IN THE PALEOARCHEAN OCEAN

Kento Motomura[1], and Shoichi Kiyokawa[1]

1. Dept. of Earth & Planetary Sciences, Kyushu Univ., Fukuoka, Japan

motomura.kento.951@m.kyushu-u.ac.jp

1. Introduction

Nitrogen is a limiting nutrient for life, and its bioavailability throughout the Earth history is crucial for understanding the biological evolution (Stüeken et al., 2016). Here we present organic carbon and nitrogen isotope data for organic matter-rich black shales of the ca. 3.2 Ga Fig Tree Group, Barberton Greenstone Belt, South Africa.

The studied section is located in the southeastern part of the Barberton Greenstone Belt, where the Fig Tree Group is well exposed along the Komati River. Black shales were collected from the ~130 m section comprising finely laminated shales and cherts.

2. Results and Discussion

In the studied section, organic carbon and nitrogen contents (TOC and TN) range from 0.1% to 5.3% and from 0.03% to 0.44%, respectively. $\delta^{13}C_{org}$ and $\delta^{15}N_{bulk}$ values are from −32.4‰ to −20.3‰ and from +1.7‰ to +8.5‰. Metamorphic effects on the $\delta^{15}N_{bulk}$ data are likely minor, based on absence of significant correlations with TN and C/N molar ratios, as well as the low metamorphic grade of the Barberton Greenstone Belt.

The positive nitrogen isotope values cannot be explained by nitrogen fixation alone since nitrogen fixation imparts an isotope fractionation of only a few permil (Stüeken et al., 2016). Hence, positive $\delta^{15}N_{bulk}$ data for the Fig Tree Group are suggestive of the development of an ocean nitrogen reservoir with an elevated nitrogen isotope composition in the ~3.2 Ga ocean.

The principal mechanism for the positive $\delta^{15}N_{bulk}$ values is still uncertain. In the modern oxic ocean, denitrification and annamox under reducing conditions at oxygen minimum zones elevate $\delta^{15}N$ values of the nitrate reservoir via preferential release of ^{14}N (Sigman et al., 2009). However, the Archean ocean is thought to have been dominantly anoxic conditions even in the surface ocean. In this case, nitrogen was likely present as ammonium rather than nitrate. If true, partial ammonium oxidation coupling with reduction of Fe oxides seems a plausible candidate for the development of the ammonium reservoir with positive $\delta^{15}N$ compositions. Interestingly, a recent Fe isotope study on the BARB 4 core containing the Fig Tree Group deposits suggests weakly oxygenated conditions of the surface ocean (Satkoski et al., 2015). If this is the case, Fe was likely oxidized above the Fe redoxcline, followed by Fe reduction coupling with oxidation of ammonium, methane, and organic matter. Importantly, black shales in the middle section are enriched in organic matter (TOC > 2%) and have low $\delta^{13}C_{org}$ and high $\delta^{15}N_{bulk}$ values ($\delta^{13}C_{org}$ < −30‰, $\delta^{15}N_{bulk}$ > +6‰) relative to the lower and upper sections ($\delta^{13}C_{org}$ ~−25‰, $\delta^{15}N_{bulk}$ ~+4‰), which is consistent with the inference. We consider that the redox cycling of Fe has resulted in the drawdown of nitrogen bioavailability and that might have been a factor buffering biological O_2 production rates.

References

Satkoski, A. M., Beukes, N. J., Li, W., Beard, B. L., & Johnson, C. M. (2015). A redox-stratified ocean 3.2 billion years ago. *Earth and Planetary Science Letters*, *430*, 43-53.

Sigman, D.M., Karsh, K.L., Casciotti, K.L., 2009. Ocean process tracers: Nitrogen isotopes in the ocean. In: Steele, J.H., Thorpe, S.A., Turekian, K.K. (Eds.), Encyclopedia of Ocean Sciences, 2nd ed. Academic press, London, pp. 40–54.

Stüeken, E. E., Kipp, M. A., Koehler, M. C., & Buick, R. (2016). The evolution of Earth's biogeochemical nitrogen cycle. *Earth-Science Reviews*, *160*, 220-239.

Boron isotope composition in tourmaline from Paleoproterozoic Pb-Zn deposits of Aravalli-Delhi Fold Belt: implications for source of ore-forming hydrothermal brines in SEDEX and MVT deposits

Niraj Bhuyan[1], Pranjit Hazarika[2], and Dewashish Upadhyay[3]

1. Department of Geology, University of Johannesburg, South Africa
   nrhuyan@uj.ac.za
2. Department of Geological Sciences, Gauhati University, India
   hazarika.pranjit@gu.ac.in
3. Department of Geology and Geophysics, Indian Institute of Technology, Kharagpur
   dewashish@gg.iitkgp.ac.in

ABSTRACT

The Aravalli Delhi Belt (ADB) in western India hosts three major base metal deposits, namely Rajpura-Dariba, Rampura-Agucha and Zawarmala. Ore mineralizations of these deposits are hosted in Paleoproterozoic volcano-metasedimentary rocks of ADFB. In this contribution, $\delta^{11}B$ of the Paleoproterozoic seawater is reconstructed by using $\delta^{11}B$ of tourmaline from Rajpura-Dariba, Zawarmala, Rampura-Agucha, Mangalwar Complex (MC) and Gangpur Schist Belt (GSB) to constrain the source of the ore-mineralizing hydrothermal fluids in SEDEX/MVT deposits. Texturally two different generations of tourmaline are identified in Rajpura-Dariba and Zawarmala deposits, i.e., Tur-I and Tu-II. Tur-I is syngenetic with ore-mineralization, while Tur-II is metamorphic. On the other hand, tourmaline identified in the Rampura-Agucha deposit represents metamorphic growth. B-isotopic compositions of syn-ore tourmaline (Tur-I) from Rajpura-Dariba and Zawarmala ranges between -18.8‰ and -16.1‰, and between -6.6‰ and -4.0‰, respectively. However, the metamorphic tourmalines from Rajpura-Dariba, Zawarmala, Rampura-Agucha, MC and GSB have $\delta^{11}B$ values ranges between -19.1 to -15.7‰, -12.4‰ to -7.7‰, -15.0‰ and -13.4‰, -15.8‰ to -14.7‰, and -12.3‰ and -11.3‰, respectively.

The $\delta^{11}B$ of metamorphic tourmaline are analyzed to estimate the $\delta^{11}B$ of the protolith of metapelite, applying P-T pseudosection modelling and mass balance calculation. Further, $\delta^{11}B$ of marine sediments were calculated to be -15.1‰ to -10.2‰, using the B-isotope fractionation factor between Miocene shale and modern clay ($\Delta^{11}B_{\text{miocene shale - modern clay}}$ = -3.8‰ to -2.2‰). Subsequently, the $\delta^{11}B$ of Paleoproterozoic seawater is estimated to be +27.3‰ to +33.4‰, using B-isotope fractionation factor between modern clay and seawater ($\Delta^{11}B_{\text{modern clay - modern seawater}}$ = -45.2‰ to -40.8‰. On comparing the $\delta^{11}B$ values syn-ore tourmalines from Rajpura-Dariba (-18.8 to -16.1‰), Zawarmala (-6.6 to -4.0‰) and global SEDEX/MVT deposits, the lighter $\delta^{11}B$ values of syn-ore tourmaline from SEDEX/MVT deposits indicate that boron required for tourmaline formation during syn-sedimentary Pb-Zn mineralization is primarily sourced from non-marine evaporites. Therefore, dissolution of non-marine evaporites in the rift settings are the major source basinal brines for the formation of ore-mineralizing fluids SEDEX/MVT deposits.

Key words: Tourmaline, SEDEX, MVT, basinal brine, ore-fluid, B-isotope, Pb-Zn mineralization

PRELIMINARY INVESTIGATION OF CU MINERALIZATION IN MATSITAMA, NORTHEASTERN BOTSWANA

Kazuyasu Shindo[1] and Thatayaone Oletile[1]

1. Department of Mineral Resources, Botswana International University of Science and Technology, Palapye, Botswana (arial 10pt font)
shindok@biust.ac.bw

1. Introduction

The Matsitama area, in northeastern Botswana is known to host Cu-mineralization. Lomberg et al. (2007) described the general geology, structure, ore and gangue minerals, and the type of deposits, present in the area. However, further research is essential to clarify the characteristics of fluids related to the Cu mineralization. Hence, we collected mineralized samples from a borehole used in the project (Lonberg et al., 2007) and investigated the mineralogy as preliminary work.

2. Geology

The Matsitama Metasedimentary Group, which is part of the Zimbabwe Craton, consists of metasedimentary rocks such as arkoses, pelites and carbonate rocks and metavolcanic rocks such as greenschist and amphibolite (Carney et al., 1994; Lomberg et al., 2007). Lintern (1982) described that the Matsitama Group has few (ultra)mafic rocks, which is different from the Tati Greenstone Belt. Coomer et al. (1977) suggested that lead was initially introduced into the sediments at 2.6-2.7 Ga. According to Lomberg et al (2007), the copper mineralization in this area is hosted in quartz-carbonate unit, with the amphibolite forming the hanging and footwall rocks.

3. Results

Sulfide minerals in the mineralized part consist of mainly chalcopyrite and minor pyrite, sphalerite, galena, bornite and pyrrhotite. Chalcopyrite is typically observed as a single phase, exhibiting anhedral shape and coexisting with bornite and sphalerite (including "chalcopyrite disease"). Figure 1 shows a photomicrograph as an example of occurrence of chalcopyrite. Pyrite grains typically show euhedral to subhedral shape and often coexist iron oxide. Furthermore, the textural relationship analysis indicate that pyrite formed before the Cu-sulfides. The gangue minerals in mineralized parts consist of mainly quartz and carbonate and trace amount of two micas (predominantly biotite and relatively minor muscovite). Grain size of quartz can reach sizes of up to 700 μm and display a bimodal distribution: (i) fine-grained aggregates (mostly < 100 μm) and (ii) coarser-grained portions (about 200 - 700 μm). Furthermore, relatively coarse quartz shows undulose extinction indicative of deformation. The carbonate, possibly calcite, has a variable grain size (up to 1mm) and occurs as aggregates coexisting with quartz.

4. Summary and next work

In the studied area copper mineralization is related to the Cu-sulfide such as chalcopyrite and bornite. These copper sulfides, as well as other sulfides, are associated with a carbonate-quartz-mica assemblage, which correlate well with the description provided by Lomberg et al. (2007). Although it is evident that hydrothermal fluid contained a certain amount of Cu, suitable for the mineralization, other characteristics of these fluids is not clear. The analysis of mineral chemistry, especially of sphalerite, along with fluid inclusion measurements, combined with sulfide assemblage, are significant for their elucidation.

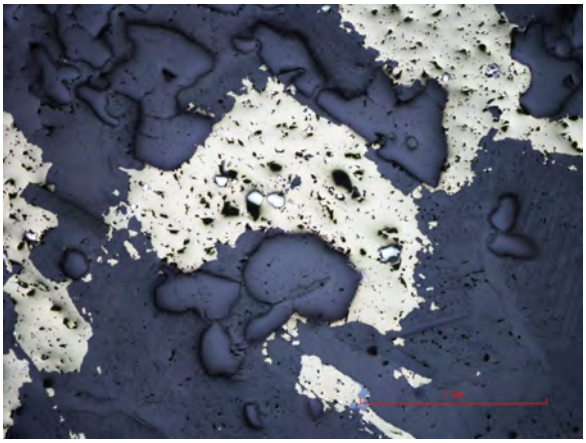

Figure 1 Chalcopyrite (Cu sulfide) in mineralized part with minor pyrite and sphalerite. Darkest gray-colored minerals are quartz and carbonate.

References

Carney, J.N., Aldiss, D.T., and Lock, N.P. (1994) *The Geology of Botswana.* Geological Survey Department, Republic of Botswana, Bulletin 37, 113p.

Coomer, P.G., Coward, M.P., and Lintern, B.C. (1977) Stratigraphy, structure and geochronology of ore leads in the Matsitama schist belt of northern Botswana. *Precambrian Research*. **5**, 23-41.

Lintern, B.C. (1982) The stratigraphy and structure of the Matsitama Schist Belt, northeastern Botswana. Unpublished PhD Thesis, Leeds University, 234p.

Lomberg, K., McKinney, M., Butcher, K., and de Visser, J. (2007) *THAKADU COPPER PROJECT Database Review, Geological Modelling and Grade Estimation of the Thakadu Copper Project*, RSG Global, 178p.

RELATIONSHIP BETWEEN LOAD CYCLE AND DEFORMATION IN SAND-WEDGE EXPERIMENTS

Satoshi Tonai[1], Nodoka Oda[1,], and Seiichiro Kanazawa[1]

1. Faculty of Science and Technology, Kochi University, Kochi, Japan
s-tonai@kochi-u.ac.jp

1. Introduction

Fold-and-thrust belts, formed by horizontal crustal shortening, are characterized by the sequential formation of multiple shear zones (Frontal Thrusts, FT) at the wedge tip during deformation. While the deformation cycle varies depending on the initial structure, understanding the underlying mechanisms is crucial for comprehending tectonic processes and material circulation within and around the wedge. However, observing the deformation cycles of natural structures, such as accretionary wedges, which span tens of thousands of years, remains challenging. As an alternative, these phenomena have often been studied through physical model experiments using dry sand (Lohrmann et al., 2003). Since 2010, studies have been examined the load cycle accompanying FT deformation (Ritter et al., 2018) and have investigated the FT formation process in detail using Digital Image Correlation (DIC) (Dotare et al., 2016).

We also conducted wedge formation experiments using layers of dry sand, aiming to understand the deformation cycle in detail by comparing synchronized load data and DIC analysis results. From these experiments, we proposed dividing one deformation cycle, indicated by the increase and decrease of loads, into four stages: Stage I, II, III, and IV. Moreover, we demonstrated that the transition from Stage III to IV and then to I occurs as newly formed FT reaches the surface. In this study, we focused on the transitions from Stage I to II and Stage II to III, aiming to understand the relationship between the entire load cycle and deformation in sand-layer wedge formation. Previous studies have often discussed sand-layer deformation based on images captured from a single direction, either lateral or overhead. In contrast, we used images captured simultaneously from both directions to extract more detailed deformation.

2. Physical model experiments

The sand-layer wedge was created by depositing Toyoura silica sand (particle size: 106–300 μm) to a thickness of 20 mm by free fall into an acrylic container lined with a sheet (width: 118 mm, length: 693 mm, height: 158 mm). The sheet was pulled horizontally at a speed of 0.125 mm/s for 250 mm, pressing the sand against a fixed wall. The deformation process was recorded at 1-second intervals using a digital camera, and the horizontal load during sheet pulling was also recorded using a load cell. A data acquisition device was used to synchronize load data with image data.

3. Results and Discussion

Using the strain analysis results of the experimental images, we examined the transition from Stage I to II. Stage I is the period after the formation of a new FT, during which the load remains constant or gradually increases. During this time, the FT of the previous generation continues to displace, albeit at a reduced speed. Stage II follows, marked by a sharp increase in load, during which the previous FT almost ceases displacement. This sequence of changes was prominently observed in the analysis results using images captured from overhead.

Similarly, we analyzed the transition from Stage II to III. During Stage III, when the load increase becomes gradual, slight strain was observed ahead of the newly displaced FT. This strain is considered a deformation zone known as the "weak shear bands" (Dotare et al., 2016), which forms just before the formation of a new FT.

By incorporating the results of this study into our previous experiments, we clarified the relationship between each stage indicated by the load cycle and deformation. This appears to be a common feature of FT formation occurring at the wedge tip.

References

Dotare et al. (2016) Initiation of a thrust fault revealed by analog experiments. *Tectonophysics* **684**, 148-156.

Lohrmann et al. (2003) The impact of analogue material properties on the geometry, kinematics, and dynamics of convergent sand wedges. *Jour. Struct. Geol.* **25**, 1691-1711.

Ritter et al. (2018) Sandbox rheometry: Co-evolution of stress and strain in Riedel– and Critical Wedge–experiments. *Tectonophysics* **722**, 400-409.

Challenges and solutions: stratigraphic delineation and sedimentological facies analysis of incised-valley fill reservoirs

A. A. Abdel Baset[1] · M. F. Abu-Hashish[2] · M. M. Abu EL-Hassan[2]

[1]El Wastani Petroleum Company (WASCO), Cairo, Egypt. [2]Department of Geology, Faculty of Science, Menoufiya University, Shibin El Kom, Egypt

1-ABSTRACT: This study addresses the challenges by integrating sedimentological facies analysis with seismic geomorphology of the Qawasim Formation, deposited during the late Messinian period. Utilizing integrated 3D seismic data, core samples, wireline logs, and borehole image logs from five wells in the Balsam field, we identify six lithofacies types within the Qawasim Formation, which are categorized into five facies associations: fluvial channels, tidally influenced fluvial channels, tidal channels, tidal bars, and tidal flats within an estuarine regime. The model identifies two primary cycles: the bottom cycle, comprising fluvial channels surrounded by overbank muds on a fluvial plain (designated as Qawasim level 1), and the top cycle, encompassing an estuarine system with tidal channels and estuarine tidal bars surrounded by tidal muds. Integrating sedimentological and seismic attributes reveals that the Qawasim Formation in the Balsam field indicates fluvial–tidal deposition within a broader estuarine context which improving hydrocarbon exploration and production strategies in the surrounding blocks of Balsam field.

INTRODUCTION: The Messinian incised-valley fills within the Nile Delta region have been highly productive in gas extraction for many years, with substantial reserves yet to be explored (Dolson et al., 2002). These formations comprise layered sequences of fluvial channels mixed with estuarine deposit sequences (Dolson et al., 2002). According to the recent study performed by Selim and Abdel Baset, (2020), the Qawasim Formation (Lower Messinian reservoir) formed from four facies associations represents the backfilling scenario within the incised-valley domain. The tectonic setting of the Balsam field significantly influenced its sedimentary deposits during the Messinian period by creating a dynamic environment conducive to incised-valley formation and sediment influx. This study aims to produce a robust geological and depositional model for the Lower Messinian section called the Qawasim Formation within the Balsam field, located inside the onshore part of the Nile Delta, the study aims to identify and classify the lithofacies within the Qawasim Formation based on a sedimentological point of view inside a broad frame of the 3D seismic data interpretation.

RESULTS: Six lithofacies 1-massive sandstone (Sm),2-cross-laminated sandstone (Sxl), 3-parallel-laminated sandstone (Sl), 4-heterolithics (HI), 5-laminated mudstone (Ml), and 6-massive mudstone (Mm), respectively. The Qawasim Formation depositional model in the Balsam field is divided into five stages. Stage 1 corresponds to a fluvial regime that followed the regional regression during the Early Messinian. Stage 2 is considered a transitional state between the fluvial and tidal regimes, which formed during the early stage of marine transgression. Stage 3, the depositional systemshifted from purely fluvial to purely estuarine. Stage 4 does not suggest any sea-levelrise due to a lateral shift from the estuarine facies. Finally, stage 5 does not represent a transgressional effect but rather the lateral shifting of the estuarine facies, resulting in tidal channels and tidal bars deposits.

CONCLUSIONS: Combining sedimentological and seismic data with petrophysical propertiescan enhance reservoir quality and performance prediction models, offering a holistic subsurface view. The insights from this study should be incorporated into field devel- opment plans, optimizing well placement and production strategies to maximize hydrocarbon recovery in the Nile Delta basin.

REFERENCES:

Dolson, J. D., El-Barkooky, A., Wehr, F., Gingerich, P., Prochazka, N., & Shann, M. (2002). The Eocene and oligocene paleo-ecology and paleo-geography of whale valley and fayoum basins: Impli- cations for hydrocarbon exploration in the Nile delta and eco- tourism in the greater fayoum basin. *AAPG International Confer-ence, 79*, 1.

Selim, S. S., & Abdel Baset, A. A. (2020). Sedimentological analysis and reservoir characterization of an estuarine bar: An example from the El-Basant Gas field, Nile Delta, Egypt. *Journal of Natu-ral Gas Science and Engineering, 84*, 103548. https://doi.org/10.1016/j.jngse.2020.103548

Face Photo

Palaeoproterozoic high $\delta^{13}C$ carbonates from the Mako Supergroup, Eastern Senegal: A first record of the Lomagundi Carbon Isotope Excursion in West Africa

Master, S.[1], Davechand, P.[2], Bekker, A.[3]

1. EGRI, School of Geosciences, University of the Witwatersrand, Johannesburg, South Africa, sharad.master@wits.ac.za
2. School of Geosciences, University of the Witwatersrand, Johannesburg, South Africa
3. Department of Earth Sciences, University of California Riverside, Riverside, CA, USA

The succession of the Palaeoproterozoic Birimian belt of the Kedougou-Kenieba Inlier of western Senegal is subdivided into the Mako and Diallé-Daléma supergroups. The c. 2.2 Ga Mako Sgp consists of tholeiitic pillow lavas overlying gabbros and ultramafic rocks. The pillow lavas are overlain by metacherts, shales, and carbonate rocks. This assemblage represents a deep-water, oceanic crust succession. It is intruded by calc-alkaline plutons, and covered by calc-alkaline lavas and pyroclastic rocks of the upper Mako Sgp, representing an oceanic island arc. The Diallé-Daléma Sgp consists of a thick (8-10 km) volcano-sedimentary succession, with calcitic and dolomitic marbles, conglomerates, breccias, greywackes, sandstones, shales, and ash beds, possibly deposited in a back-arc basin [1].

Carbonate rocks of the Mako Supergroup lie directly above tholeiitic pillow lavas, with associated banded cherts and some thin organic-rich black shales. These rocks also include hyaloclastic breccias, containing angular fragments of vesicular basalt, formed by explosive eruption of basalt on the seafloor and enclosed in a carbonate matrix. The Mako Sgp carbonates are mainly dolomitic marbles with minor calcitic marbles. Their C isotopic composition shows δ13 C values ranging between +7.9 and +11.2 ‰ V-PDB (n = 18), indicating that these carbonates were deposited during the Lomagundi Carbon Isotope Excursion (LCIE) in seawater composition between c. 2.2 and 2.06 Ga, recorded by high δ13 C values of sedimentary carbonates with this age [2]. Their stratigraphic position and high δ13 C values are similar to those of marbles associated with seafloor pillow lavas in the Ruwenzori Belt, Uganda [3]. Although the isotopic systems have been disturbed by metamorphism, as shown by large variations in δ18 O and Mn/Sr values, the high δ13 C values indicate a source from 13 C-enriched seawater. The sedimentary carbonates of the Mako Sgp have a tentative Pb-Pb age of 2.15 Ga [4]. They overlie pillow lavas, which have yielded age of c. 2.197 Ga [5], and, since they display the LCIE, their age is constrained between c. 2.2 and 2.06 Ga. In contrast, metacarbonates from two quarries near Ibel, located in the Diallé-Daléma Supergroup, consist of highly deformed calcitic and ferroan, dolomitic marbles, with δ13 C values ranging between -1.9 and +2.5 ‰ V-PDB (n = 30). These δ13 C values are within the range of normal marine carbonates, and are similar to previously reported δ13 C values of the Diallé-Daléma Sgp metacarbonates from Ylimalo along the Falémé River, ranging from +0.3 to +1.7 ‰ V-PDB (n = 4) [6]. The Diallé-Daléma Sgp metacarbonates have a Pb-Pb age of 2065 ± 33 Ma [7]. Since they postdate the LCIE, their depositional age is likely to be in the range 2060-2030 Ma.

References

[1] Master, S. 1993. CIFEG Occ. Publ. 1993/23, Orléans, 76-81. [2] Karhu, J.A., Holland, H.D., 1996, Geology, 24(10), 867-870. [3] Master, S. et al., 2013. Chem. Geology, 362, 157-164. [4] Diallo, D.P. et al., 1993, CIFEG Occ. Publ 1993/23, 11-15. [5] Dia, A. et al., 1997. J. Afr. Earth Sci., 24(3), 197-213. [6] Master, S. et al., 1993. CIFEG Occ. Publ, 1993/23, 38-41. [7] Vialette, Y. et al., 1990. Abstr. CAG15, CIFEG Occ. Publ, 1990/20, p. 51.

Timetable


2024 Dec. 5
9:00
9:10
9:20
9:30
9:40
9:50
10:00
10:10
10:20
10:30
10:40
10:50
11:00
11:10
11:20
11:30
11:40
11:50
12:00
1 Axel Hofmann
2 Andrew Kennedy
3 Anna Molekwa
4 Hanna ELDOKOUNY
5 Mahyra Tedeschi
6 Tathagata Chowdhury
7 Koki Maegawa
8 Fezeka Dliwako
poster
Lunch
13:50
14:00
14:10
14:20
14:30
14:40
14:50
15:00
15:10
15:20
15:30
15:40
15:50
16:00
16:10
16:20
16:30
16:40
16:50
17:00
17:10
9 Manuel Reinhardt
10 Thatayaone Oletile
11 Isaac Ajigo
12 Shoichi Kiyokawa
13 Carlos Alberto Rosière
14 Fatma Abdelgalil E.. Mousa
15 Maher Dawoud
2024 Dec. 6
9:00
9:10
9:20
9:30
9:40
9:50
10:00
10:10
10:20
10:30
10:40
10:50
11:00
11:10
11:20
11:30
11:40
11:50
12:00
16 Frank NYAME
17 Kwabina Ibrahim
18 Samuel Nunoo
19 Satoshi Yoshimaru
20 Kwame Fynn
21 Ion FRANCOVSCHI
Lunch
13:50
14:00
14:10
14:20
14:30
14:40
14:50
15:00
15:10
15:20
15:30
15:40
15:50
16:00
16:10
16:20
16:30
16:40
16:50
17:00
17:10
17:20
22 Andrey Bekker
23 Kento Motomura
24 Niraj Buhyan
25 Kazuyasu Shindo
26 Satoshi Tonai
27 MOHAME ABOUELHASSAN
28 Sharad Master